23. Sjöström A, et al. (2001) Acquisition of external major histocompatibility complex class I molecules by natural killer cells expressing inhibitory Ly49 receptors. *J Exp Med* 194:1519–1530.
24. Smyth MJ, Hayakawa Y, Takeda K, Yagita H (2002) New aspects of natural-killer-cell surveillance and therapy of cancer. *Nat Rev Cancer* 2:850–861.
25. Homann D, et al. (2002) CD40L blockade prevents autoimmune diabetes by induction of bitypic NK/DC regulatory cells. *Immunity* 16:403–415.
26. Pillarisetty VG, Katz SC, Bleier JI, Shah AB, Dematteo RP (2005) Natural killer dendritic cells have both antigen presenting and lytic function and in response to CpG produce IFN-γ via autocrine IL-12. *J Immunol* 174:2612–2618.
27. Taieb J, et al. (2006) A novel dendritic cell subset involved in tumor immunosurveillance. *Nat Med* 12:214–219.
28. Chan CW, et al. (2006) Interferon-producing killer dendritic cells provide a link between innate and adaptive immunity. *Nat Med* 12:207–213.
29. Qureshi OS, et al. (2011) Trans-endocytosis of CD80 and CD86: A molecular basis for the cell-extrinsic function of CTLA-4. *Science* 332:600–603.
30. Cosgrove D, et al. (1991) Mice lacking MHC class II molecules. *Cell* 66:1051–1066.
31. Ogasawara K, et al. (2003) Impairment of NK cell function by NKG2D modulation in NOD mice. *Immunity* 18(1):41–51.
32. Nakayama M, et al. (2009) Tim-3 mediates phagocytosis of apoptotic cells and cross-presentation. *Blood* 113:3821–3830.
33. Nakayama M, et al. (2007) Paired Ig-like receptors bind to bacteria and shape TLR-mediated cytokine production. *J Immunol* 178:4250–4259.

THE JOURNAL OF IMMUNOLOGY

High Clonality of Virus-Specific T Lymphocytes Defined by TCR Usage in the Brains of Mice Infected with West Nile Virus

Kazutaka Kitaura, Yoshiki Fujii, Daisuke Hayasaka, Takaji Matsutani, Kenji Shirai, Noriyo Nagata, Chang-Kweng Lim, Satsuki Suzuki, Tomohiko Takasaki, Ryuji Suzuki and Ichiro Kurane

J Immunol 2011; 187:3919-3930; Prepublished online 9 September 2011;
doi: 10.4049/jimmunol.1100442
http://www.jimmunol.org/content/187/8/3919

The Journal of Immunology is published twice each month by
The American Association of Immunologists, Inc.,
9650 Rockville Pike, Bethesda, MD 20814-3994.

Print ISSN: 0022-1767 Online ISSN: 1550-6606.

High Clonality of Virus-Specific T Lymphocytes Defined by TCR Usage in the Brains of Mice Infected with West Nile Virus

Kazutaka Kitaura,*,†,‡ Yoshiki Fujii,*,† Daisuke Hayasaka,§ Takaji Matsutani,¶ Kenji Shirai,*,†,‡ Noriyo Nagata,‖ Chang-Kweng Lim,† Satsuki Suzuki,# Tomohiko Takasaki,† Ryuji Suzuki,* and Ichiro Kurane†,‡

It has been reported that brain-infiltrating T lymphocytes play critical roles in the clearance of West Nile virus (WNV) from the brains of mice. We characterized brain-infiltrating T lymphocytes by analyzing the TCR α- and β-chain repertoires, T cell clonality, and CDR3 sequences. $CD3^+CD8^+$ T cells were localized in the WNV-infected brains. The expression of CD3, CD8, CD25, CD69, perforin, and granzymes positively correlated with viral RNA levels, and high levels of expression of IFN-γ, TNF-α, and IL-2 were detected in the brains, suggesting that Th1-like cytotoxic $CD8^+$ T cells are expanded in the brains in response to WNV infection. The brain-infiltrating T lymphocytes dominantly used TCR genes, VA1-1, VA2-1, VB5-2, and VB8-2, and exhibited a highly oligoclonal TCR repertoire. Interestingly, the brain-infiltrating T lymphocytes had different patterns of TCR repertoire usages among WNV-, Japanese encephalitis virus-, and tick-borne encephalitis virus-infected mice. Moreover, $CD8^+$ T cells isolated from the brains of WNV-infected mice produced IFN-γ and TNF-α after in vitro stimulation with peritoneal cells infected with WNV, but not with Japanese encephalitis virus. The results suggest that the infiltrating $CD8^+$ T cells were WNV-specific, but not cross-reactive among flaviviruses. T cells from the WNV-infected brains exhibited identical or similar CDR3 sequences in TCRα among tested mice, but somewhat diverse sequences in TCRβ. The results indicate that WNV-specific $CD3^+$ $CD8^+$ T cells expanding in the infected brains are highly oligoclonal, and they suggest that TCR α-chains play a dominant and critical role in Ag specificity of WNV-specific T cells. *The Journal of Immunology*, **2011, 187: 3919–3930.**

West Nile virus (WNV) is a member of the Flaviviridae family and causes a range of illnesses from mild fever to acute flaccid paralysis and lethal encephalitis in humans. Approximately 20–30% of infected individuals develop flu-like clinical manifestations characterized as West Nile fever, and about 1 in 150 cases is accompanied by severe neurologic disease, such as cognitive dysfunction, ocular manifestations, meningitis, encephalitis, and flaccid paralysis (1–3). West Nile fever was endemic in the Middle East, Europe, and Africa before the mid-1990s, but has since spread throughout the world, including the Americas (4). However, vaccines or specific therapies for WNV are unavailable for humans. Moreover, the pathogenesis of WNV encephalitis is not clear, especially the reasons why most of the symptomatic cases demonstrate acute febrile illness but some develop severe encephalitis.

$CD8^+$ cytotoxic T cells play essential roles in controlling WNV infection (5) and protection against WNV encephalitis (6). Previously, we have demonstrated the existence of Ag-specific T cells in the brains of C3H mice infected with Japanese encephalitis virus (JEV), which is closely related to WNV (7). In mice infected with flaviviruses, Ag-specific T lymphocytes infiltrating into the CNS mediate the clearance of virus, preventing encephalitis. However, little information regarding Ag specificity and diversity of the CNS-infiltrating T cells is available. Immune responses against virus infections are initiated by specific recognition of a viral Ag presented on an MHC by a TCR. Functional TCR α- and β-chains genes are generated by somatic gene rearrangements of germline-encoded V(D)J and constant gene segments. The Ag specificity and diversity of the TCR depends mainly on CDR3, formed by nucleotide addition/insertion during the gene rearrangements (8) that contact directly with an Ag peptide on MHC (9). Many investigations with quantitative and qualitative analyses of TCR repertoires and CDR3 sequences have contributed to the elucidation of pathological conditions and/or immunological dynamics in infectious disease research (7), pathogenesis of autoimmune diseases (10–12), and/or physiological analysis (13, 14). Additionally, neutralizing Abs induced by WNV partially protect against JEV infection (15). The immunological cross-reaction between closely related flaviviruses raised the question of whether

*Department of Rheumatology and Clinical Immunology, Clinical Research Center for Allergy and Rheumatology, Sagamihara National Hospital, National Hospital Organization, Kanagawa 228-0815, Japan; †Department of Virology 1, National Institute of Infectious Diseases, Tokyo 162-8640, Japan; ‡Department of Infection Biology, Institute of Basic Medical Sciences, University of Tsukuba, Ibaraki 305-8575, Japan; §Department of Virology, Institute of Tropical Medicine, Nagasaki University, Nagasaki 852-8523, Japan; ¶Laboratory of Immune Regulation, Wakayama Medical University, Osaka, 567-0085, Japan; ‖Department of Pathology, National Institute of Infectious Diseases, Tokyo 208-0011, Japan; and #Section of Biological Science, Research Center for Odontology, Nippon Dental University School of Life Dentistry at Tokyo, Tokyo 102-8159, Japan

Received for publication February 14, 2011. Accepted for publication July 27, 2011.

This work was supported in part by Grants-in-Aid for Research on Emerging and Re-emerging Infectious Diseases from the Ministry of Health, Labor, and Welfare, Japan (Grants H20-shinkou-ippan-013 and H20-shinkou-ippan-015) as well as by Grant-in-Aid for Challenging Exploratory Research 23659237 from the Japan Society for the Promotion of Science.

Address correspondence and reprint requests to Dr. Ichiro Kurane, Department of Virology 1, National Institute of Infectious Diseases, 1-23-1 Toyama, Shinjuku-ku, Tokyo 162-8640, Japan. E-mail address: kurane@nih.go.jp

Abbreviations used in this article: BSL, biosafety level; IHC, immunohistochemical; JEV, Japanese encephalitis virus; MCA, TCR α-chain C region-specific primer; MCB, TCR β-chain C region-specific primer; PEC, peritoneal cell; qPCR, quantitative real-time RT-PCR; TBEV, tick-borne encephalitis virus; TCRAV, TCR α-chain variable; TCRBV, TCR β-chain variable; TCRV, TCR V region; WNV, West Nile virus.

www.jimmunol.org/cgi/doi/10.4049/jimmunol.1100442

brain-infiltrating T lymphocytes use identical or similar TCR repertoires among these closely related flaviviruses.

To characterize the brain-infiltrating T lymphocytes in WNV-infected mice, we performed immunohistochemical (IHC) and quantitative real-time RT-PCR (qPCR) analyses for T cell-related surface molecules, cytokines, chemokines, and cytotoxic granules. The results demonstrated that Th1-like cytotoxic $CD8^+$ T cells accumulated in the brains. Next, to disclose Ag specificity and diversity in the brain-infiltrating T lymphocytes, we analyzed the TCR repertoires and TCR clonotypes in the brains of mice infected with WNV, JEV, and tick-borne encephalitis virus (TBEV). The results indicated that T cells accumulated in the mice brains had a distinct TCR repertoire among WNV, JEV, and TBEV and exhibited high oligoclonality. Furthermore, we performed in vitro stimulation assays by coculturing T cells isolated from WNV-infected mouse brains with peritoneal cells (PECs) obtained from different strains of mice that were infected with either WNV or JEV. These T cells produced IFN-γ and TNF-α in response to WNV-infected PECs with a syngeneic MHC haplotype. The present study provides important information about the Ag specificity and diversity of brain-infiltrating T lymphocytes in flavivirus-infected mice.

Materials and Methods

Virus

The NY99-6922 strain of WNV (GenBank accession no. AB185915; http://www.ncbi.nlm.nih.gov/genbank and the JaTH160 strain of JEV (GenBank accession no. AB269326) were used in this study. The WNV was prepared from the conditioned medium of Vero cells that were infected with a previously prepared virus stock (15). Vero cells were maintained in Eagle's MEM (Nissui Pharmaceutical, Tokyo, Japan) containing 10% FCS. The virus titer was 1.4×10^5 PFU/ml. JEV was prepared as described previously (7) with a virus titer of 1×10^{10} PFU/ml. The experiments using live viruses were performed in a biosafety level (BSL) 3 laboratory of the National Institute of Infectious Diseases, Japan, according to standard BSL3 guidelines. The Oshima 5-10 strain of TBEV (GenBank accession no. AB062063) (16) was also used in this study. The virus was prepared from the conditioned medium of baby hamster kidney cells infected with a previously prepared virus stock (17). Baby hamster kidney cells were maintained in Eagle's MEM containing 8% FCS. Experiments using live TBEV were performed in a BSL3 laboratory of the Tokyo Metropolitan Institute for Neuroscience according to standard BSL3 guidelines.

Mice

C3H/HeNJcl (H-2^k), C57BL/6JJcl (H-2^b), and BALB/cAJcl (H-2^d) female mice were purchased from CLEA Japan (Tokyo, Japan) and kept in a specific pathogen-free environment. All animal experiments were done according to the relevant ethical requirements and with approval from the committees for animal experiments at the National Institute of Infectious Diseases and the Tokyo Metropolitan Institute for Neuroscience, Japan.

Virus challenges

Seven-week-old C3H/HeNJcl female mice were injected i.p. with the $30 \times LD_{50}$ (1.3×10^3 PFU/0.5 ml) WNV and the $100 \times LD_{50}$ (1.2×10^4 PFU/0.5 ml) JEV or PBS alone (mock infection). Four, 7, and 10 days later, WNV-infected mice were sacrificed under general anesthesia. Ten days later, JEV-infected mice were sacrificed under general anesthesia. In TBEV infection, 7-wk-old C3H/HeNJcl female mice were injected s.c. with 1.0×10^3 PFU/0.5 ml TBEV or PBS. Thirteen days later, mice were sacrificed under general anesthesia.

Histological and IHC analyses

Brains were excised for use in histological and IHC examinations. Tissue samples were fixed overnight at 4°C with paraformaldehyde-lysine-periodate, washed with PBS, and immersed in 5% sucrose/PBS for 1 h, in 15% sucrose/PBS for 3 h, and in 30% sucrose/PBS overnight at 4°C. Samples were embedded in Tissu Mount (Chiba Medical, Saitama, Japan) and quick-frozen in a mixture of acetone and dry ice. For histochemical staining, 6-μm cryosections were air-dried on poly-L-lysine–coated glass slides and were stained with H&E. For IHC analyses, cryosections were stained with anti-mouse CD3ε (145-2C11; BD Pharmingen, San Diego, CA), CD4 (GK5.1; BD Pharmingen), and CD8α (53-6.7; BD Pharmingen) mAbs. In short, glass slides were overlaid with PBS containing blocking reagents (a 1:20 dilution of normal goat serum or normal rabbit serum, 0.025% Triton X-100 [Wako Pure Chemicals, Osaka, Japan], and 5% BSA [Sigma-Aldrich, St. Louis, MO]) and incubated for 30 min at room temperature. The mAbs were loaded onto the glass slides and incubated for 1 h at room temperature. After washing with PBS (three times for 5 min), each section was treated with a secondary Ab (biotinylated goat anti-hamster IgG Ab or biotinylated rabbit anti-rat IgG Ab) at room temperature for 1 h and then with avidin–biotin complex for 30 min, followed by 3,3′-diaminobenzidine staining (0.06% 3,3′-diaminobenzidine, 0.03% H_2O_2 in 0.1 M Tris-HCl buffer [pH 7.6]; Wako Pure Chemicals). Finally, the glass slides were counterstained with hematoxylin to visualize nuclei.

Isolation of total RNA from tissues

Fresh brains and spleens infected with WNV or TBEV were excised intact and immediately submerged in RNAlater RNA stabilization reagent (Qiagen, Hilden, Germany) (18). Total RNA was isolated using the RNeasy Lipid Tissue Mini Kit (Qiagen) according to the manufacturer's instructions.

Quantitative estimation of the expression of immune-related genes and WNV RNA in brains and spleens

Expression levels of mRNA for immune-related genes including T cell-related CD Ags, cytokines, chemokines, chemokine receptors, and cytotoxic granules were measured by qPCR using a LightCycler apparatus (Roche Diagnostics, Basel, Switzerland). Previously demonstrated primer pairs specific for GAPDH, CD3, CD4, CD8, IFN-γ, TNF-α, IL-2, IL-4, IL-5, CCL5, CXCL10, and CXCR3 were used in this study (7, 19). Other primer pairs (CCR5, perforin, granzyme A, granzyme B, CD25 [IL-2Rα], and CD69) were designed for this study (Table I). IL-10–specific primers were purchased from Takara Bio (Otsu, Japan). Freshly isolated RNA from the spleens and brains of WNV- or mock-infected mice ($n = 5$) was converted to cDNA using a PrimeScript RT reagent kit (Takara Bio) according to the manufacturer's instructions. The PCR reaction was performed using SYBR Premix TaqII (Takara Bio) for SYBR Green I and was carried out in a 20-μl volume containing 2 μl cDNA template originating from 50 ng total RNA, 0.4 μl each 10 μM forward and reverse primers, and 10 μl SYBR Premix TaqII. After an initial denaturation step at 95°C for 10 s, temperature cycling was initiated. Each cycle consisted of 95°C for 5 s and 60°C for 30 s, and the fluorescence was read at the end of this second step. In total, 40 cycles for GAPDH and 50 cycles for other primer sets were performed accordingly. Melting curve analysis was performed immediately after amplification at a linear temperature transition rate of 0.1°C/s from 65°C to 95°C with continuous fluorescence acquisition. The absolute copy number of each gene was calculated by using a standard curve generated by serial dilution of the recombinant plasmid DNA encoding gene of interest, ranging from 10^1 to 10^8 copies. Calculated copy numbers were normalized based on the copy numbers of the housekeeping gene GAPDH.

Table I. Sequences of qPCR primers

Targets	Forward Primer (5′–3′)	Reverse Primer (5′–3′)
CCR5	ATATGCAAAGGGACGGACAC	GCAAGAAGCGACTTTATGGC
IL-10	GACCAGCTGGACAACATACTGCTAA	GATAAGGCTTGGCAACCCAAGTAA
Perforin	GCCTGGTACAAAAACCTCCA	AGGGCTGTAAGGACCGAGAT
Granzyme A	CCTGAAGGAGGCTGTGAAAG	GAGTGAGCCCCAAGAATGAA
Granzyme B	CCATCGTCCCTAGAGCTGAG	TTGTGGAGAGGGCAAACTTC
CD25	AAGATGAAGTGTGGGAAAACGG	GGGAAGTCTGTGGTGGTTATGG
CD69	AGGATCCATTCAAGTTTCTATCCC	CAACATGGTGGTCAGATGATTCC

The viral RNA levels of WNV were examined with envelope-specific forward and reverse primers (5′-TCAGCGATCTCTCCACCAAAG-3′ and 5′-GGGTCAGCACGTTTGTCATTG-3′) and a dual fluorophore-labeled probe (5′-CFSE-TGCCCGACCATGGGAGAAGCTC-TAMRA-3′) using a Prism 7000 sequence detection system (Applied Biosystems, Foster, CA). A TaqMan Ez RT-PCR kit (Applied Biosystems) was used according to the manufacturer's instructions. A total reaction mixture of 25 μl containing 50 ng total RNA was incubated at 48°C for 30 min for reverse transcription and then at 95°C for 10 min for inactivation of reverse transcriptase and initial denaturation. PCR was carried out for 40 cycles at 95°C for 15 s and 57°C for 1 min, and the fluorescence was read at the final PCR round. The copy number of each sample was determined on the basis of a standard curve created with a serial dilution of in vitro-synthesized WNV RNA ranging from 10^1 to 10^8 copies, provided by Dr. Soichi Nukuzuma (Kobe Institute of Health, Kobe, Hyogo, Japan).

TCR repertoire analysis

TCR repertoire analysis was performed with WNV- and TBEV-infected mice samples (n = 5) by an adaptor ligation-mediated PCR and microplate hybridization assay method (20–22). Briefly, isolated total RNA was converted to double-stranded cDNA using a SuperScript cDNA synthesis kit (Invitrogen, Carlsbad, CA) according to the manufacturer's instructions, except that a specific primer (BSL-18E) was used (22). The P10EA/P20EA adaptors were ligated to the 5′ end of the cDNA and this adaptor-ligated cDNA was cut with SphI. PCR was performed with TCR α-chain C region-specific (MCA) 1 or TCR β-chain C region-specific primers (MCB) 1 and P20EA. The second PCR was performed with MCA2 or MCB2 and P20EA. The third PCR was performed using both P20EA and 5′-biotinylated MCA3 or MCB3 primer for biotinylation of PCR products.

Ten picomoles of amino-modified oligonucleotides specific for the TCR α-chain variable (TCRAV) and TCR β-chain variable (TCRBV) segments were immobilized onto carboxylate-modified 96-well microplates with water-soluble carbodiimide. Prehybridization and hybridization were performed in GMCF buffer (0.5 M Na_2HPO_4 [pH 7.0], 1 mM EDTA, 7% SDS, 1% BSA, and 7.5% formamide) at 47°C. One hundred microliters of the denatured 5′-biotinylated PCR products was mixed with the equivalent volume of 0.4 N NaOH/10 mM EDTA, and the mixture was added to 10 ml GMCF buffer. One hundred microliters of hybridization solution was used in each well of the microplate containing immobilized oligonucleotide probes specific for V segments. After hybridization, wells were washed four times with washing buffer (2× SSC, 0.1% SDS) at room temperature. Plates were then incubated at 37°C for 10 min for stringency washing. After washing four times with the same washing buffer, 200 μl TB-TBS buffer (10 mM Tris-HCl, 0.5 M NaCl [pH 7.4], 0.5% Tween 20, and 0.5% blocking reagent; Roche Diagnostics) was added to block nonspecific binding. Next, 100 μl 1:2000 diluted alkaline phosphatase-conjugated streptavidin in TB-TBS was added, and the sample was incubated at 37°C for 30 min. Plates were washed six times in T-TBS (10 mM Tris-HCl, 0.5 M NaCl [pH 7.4], 0.5% Tween 20). For color development, 100 μl substrate solution (4 mg/ml p-nitrophenylphosphate [Sigma Aldrich] in 10% diethanolamine [pH 9.8]) was added, and absorbance was determined at 405 nm. The ratio of the hybridization intensity of each TCR V region (TCRV)-specific probe to that of a TCR C region-specific probe (V/C value) was determined using the TCR cDNA concentrated samples that contained the corresponding TCRV segment and the universal TCR constant segment, respectively. Absorbance obtained with each TCRV-specific probe was divided by the corresponding V/C value. The relative frequency was calculated based on the corrected absorbances using the formula: relative frequency (%) = (corrected absorbance of TCRV-specific probe/sum of corrected absorbances of TCRV-specific probes) × 100.

T cell clonality analysis with CDR3 size spectratyping

The level of T cell clonality was evaluated in samples from WNV- and TBEV-infected mice (n = 5) using a CDR3 size spectratyping method (23). PCR was performed for 30 cycles in a 20 μl volume under the same conditions as described above. The PCR mixture consisted of 1 μl 1:20 or 1:50 diluted second PCR product, 0.1 μM 5′-Cy5 MCA3/MCB3 primer, and 0.1 μM primer specific for each variable segment. Two microliters 1:20 diluted PCR product was analyzed with the CEQ8000 genetic analysis system (Beckman Coulter, Fullerton, CA). The spleens of mock-infected mice were used as normal controls showing a Gaussian distribution pattern with multiple peaks.

Determination of CDR3 nucleotide sequences

PCR was performed with 1 μl 1:20 diluted second PCR product, using a forward primer specific for the V region and a reverse primer specific for the C region (MCA4 or MCB4) under the conditions described above. The primers used in this study were as follows: VA1-1, 5′-AGACTCCCAGCCCAGTGACT-3′; VA2-1, 5′-TGCAGTTATGAGGACAGCACTT-3′; VB5-2, 5′-GGATTCCTACCCAGCAGATTC-3′; and VB8-2, 5′-GGCTACCCCCTCTCAGACAT-3′. After elution from agarose gels, PCR products were cloned into the pGEM-T Easy Vector (Promega, Madison, WI). The recombinant plasmid DNA was transfected into DH5α competent cells. Sequence reactions were performed with the GenomeLab DTCS Quick Start Kit (Beckman Coulter) and analyzed by the CEQ8000 genetic analysis system (Beckman Coulter). In total, 64 clones from each sample of WNV- and TBEV-infected mouse brains (n = 5) were examined in this experiment.

In vitro stimulation of T cells from WNV-infected mouse brain

WNV- or JEV-infected C3H/HeN mice (n = 8) were sacrificed under general anesthesia on day 10 postinfection, and brains were removed. Brains were kept on ice in RPMI 1640 containing 10% FCS and homogenized gently by pressing through a 100-μm mesh tissue strainer (BD Pharmingen). Homogenates were then centrifuged at 400 × g for 10 min, and cell pellets were resuspended in 5 ml RPMI 1640 and layered over 5 ml Lympholyte-M (Cedarlane Laboratories, Hornby, ON, Canada) before centrifugation at 1000 × g for 20 min at 22°C. Next, the isolated lymphocyte pool was washed twice and resuspended in MACS buffer (Ca^{+}- and Mg^{+}-free PBS, 2 mM EDTA, and 0.5% BSA) and incubated with anti-CD4 and/or anti-CD8 MACS beads (Miltenyi Biotec, Auburn, CA) at 4°C for 15 min. Cell suspensions were diluted 20 times in

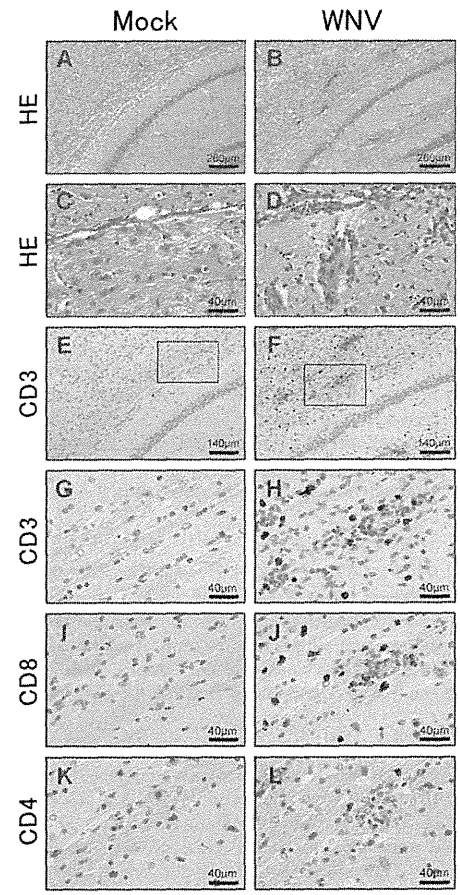

FIGURE 1. Histopathological study and IHC analysis of $CD3^{+}$, $CD8^{+}$, and $CD4^{+}$ cells in WNV-infected mouse brain. Representative photomicrographs of brain sections from mock-infected or WNV-infected mice at day 10 postinfection, stained with H&E (*A–D*) and CD3, CD4, and CD8 (*E–L*). Neuronal degeneration and inflammatory cell infiltration in hippocampus and perivascular areas are shown in WNV-infected mouse brains, but not those of mock-infected mice. For the IHC analysis, the localization of $CD3^{+}$ and $CD8^{+}$ cells is shown throughout the brain of WNV-infected mice, but not those of mock-infected mice (*E–J*). Alternatively, $CD4^{+}$ cells were detected sporadically in both WNV- and mock-infected mice (*K*, *L*). The area of higher magnifications (original magnification ×3.5) are indicated by the black boxes in *E* and *F*.

MACS buffer and centrifuged at 300 × *g* for 10 min. Cell pellets were resuspended in MACS buffer and filtered through MACS LS separation columns (Miltenyi Biotec), according to the manufacturer's protocol. Collected $CD4^+$ and/or $CD8^+$ cells were resuspended in RPMI 1640 containing 10% FCS and antibiotics (assay medium), adjusted to 2.5×10^6 cells/ml, and were used in in vitro stimulation assays. PECs were collected in 10 ml cold Ca^{+}- and Mg^{+}-free PBS, from C3H/HeN, C57BL/6j, and BALB/c mice ($n = 3$) after scarifying the mice under general anesthesia. The cells were centrifuged at 600 × *g* for 5 min, resuspended in assay medium, and counted. After infection with WNV or JEV at a multiplicity of infection of 100 PFU/cell at 37°C in 5% CO_2 for 60 min, the cells were washed twice with assay medium. The concentration of PECs was adjusted to 5.0×10^5 cells/ml, and 100 μl PEC was dispensed into flat-bottom 96-well trays (Nunc, Roskilde, Denmark). Subsequently, 100 μl 2.5×10^5 T cells from WNV- or JEV-infected C3H mouse brains was added and cultured at 37°C in 5% CO_2 for 12 h. Culture supernatant fluids were collected, and levels of IFN-γ and TNF-α were measured by ELISA (MIF00 and MTA00, respectively; R&D Systems, Minneapolis, MN) according to the manufacturer's instructions. Cells were then further cultured for 3 d and used for CDR3 analysis.

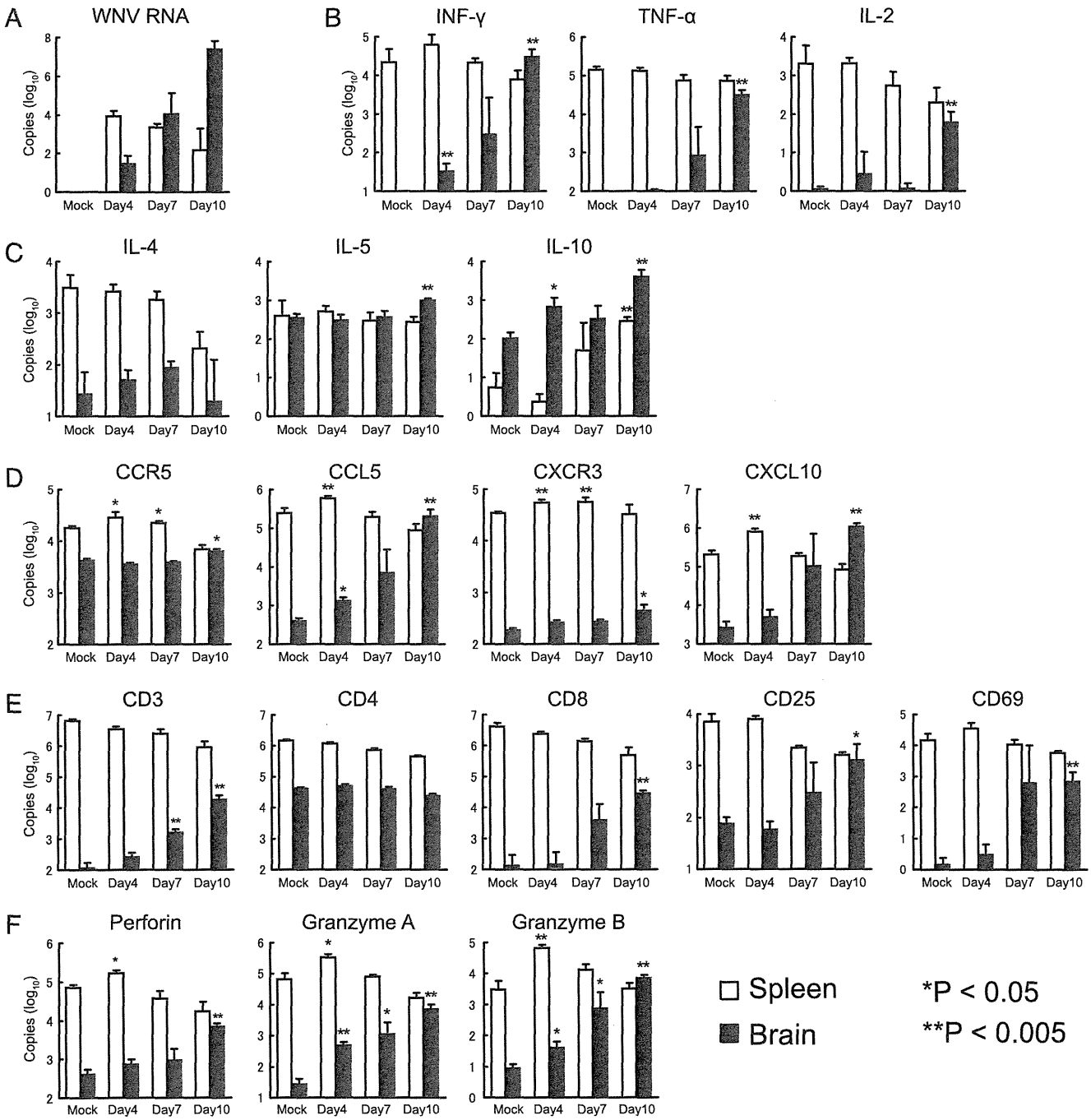

FIGURE 2. Quantification of WNV RNA and of T cell immune-related gene mRNAs by qPCR. Copy number of WNV RNA (*A*), the mRNA expression level of IFN-γ, TNF-α, and IL-2 as Th1-type cytokines (*B*), IL-4, IL-5, and IL-10 as Th2 type cytokines (*C*), CCR5, CCL5, CXCR3, and CXCL10 as chemokines and chemokine receptors (*D*), CD3, CD4, CD8, CD25 (IL-2R), and CD69 as T cell-related Ags (*E*), and perforin, granzyme A, and granzyme B as cytotoxic granules (*F*) are shown. The copy numbers per 50 ng total RNA were calibrated with GAPDH expression, except that WNV RNA was calculated from the standard density of in vitro-synthesized WNV RNA. RNA was extracted from spleens (open bars) or brains (filled bars) of mock-infected mice (Mock) or WNV-infected mice at 4, 7, and 10 d after virus inoculation. Open or filled bars and vertical error bars indicate mean ± SD of five mice. Significant differences are shown when compared with mock spleen or brain using a Student unpaired *t* test (*$p < 0.05$, **$p < 0.005$). All experiments were performed in triplicate.

Statistical analysis

Differences were statistically analyzed by a Student unpaired t test using StatView 5.0 for Windows (SAS Institute, Cary, NC). A p value <0.05 was determined to be statistically significant. Moreover, to assess biologically significant differences, a 5% cut-off threshold was added for TCR repertoires.

Results

Histopathological study of brains from WNV-infected mice

Brains were removed from WNV- or mock-infected mice 10 d postinfection and prepared for histopathological examinations as described in *Materials and Methods*. Representative histological changes are shown in Fig. 1*A–D*. Severe neuronal degeneration and inflammatory cell infiltration were detected in the brains from infected mice, especially in the hippocampus, perivascular tissue, and cerebral meninges. In WNV-infected mouse brains, but not in mock-infected mouse brains, $CD3^+$ and $CD8^+$ T cells were also widely detected, especially in the cerebral meninges, perivascular tissue, and hippocampus (Fig. 1*E–J*). $CD4^+$ cells were detected in brain sections both from WNV- and mock-infected mice (Fig. 1*K*, 1*L*).

Propagation of WNV and cytokine expression in brains from WNV-infected mice

The amount of WNV RNA in brains and spleens was measured by qPCR after i.p. inoculation of the virus (Fig. 2*A*). WNV RNA was first detected on day 4 in both organs. RNA levels increased largely with time in the brains, whereas they gradually decreased after day 4 in the spleens. Cytokine expression in the brains of WNV-infected mice was also measured (Fig. 2*B*, 2*C*). A temporal increase in the expression of IFN-γ, TNF-α, and IL-2 was detected in the brains of the WNV-infected mice, but not in those of mock-infected ones. IL-4, IL-5, and IL-10 expression was detected in the brains of mock-infected mice. The expression levels of IL-5 increased significantly on day 10 in WNV-infected mice. The expression of IL-10 increased on day 4 in the brains and slowly in the spleens following WNV infection. The expression levels of chemokines (CCL5 and CXCL10) and chemokine receptors (CCR5 and CXCR3) considerably increased in the brains after WNV infection (Fig. 2*D*). In particular, the expression levels of CCL5 and CXCL10 were increased >100-fold on day 10 compared with day 4. These results indicated that expression

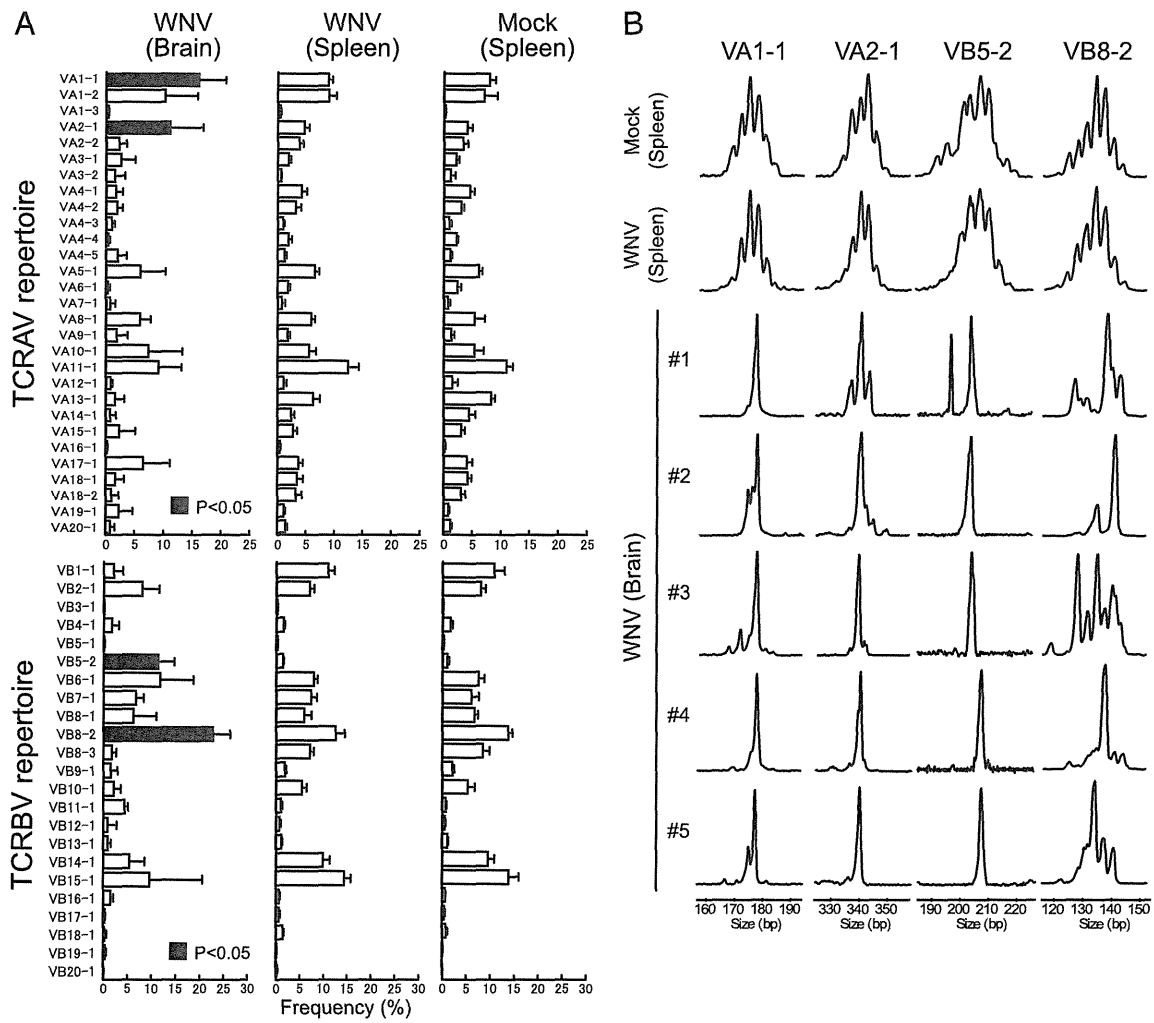

FIGURE 3. TCR repertoire analysis and CDR3 size spectratyping in spleens and brains of WNV-infected mice. *A*, TCRAV and TCRBV repertoires were analyzed by microplate hybridization assay method. The open or filled bars and horizontal bars indicate mean ± SD of frequencies in five mice. In the brains of WNV-infected mice on day 10, percentage frequencies of T cells bearing VA1-1, VA2-1, VB5-2, and VB8-2 were significantly increased compared with those of mock-infected mouse spleens ($p < 0.05$, Student unpaired t test, filled bars). All experiments were performed in triplicates. *B*, CDR3 size spectratyping patterns of VA1-1, VA2-1, VB5-2, and VB8-2 in five mice infected with WNV on day 10. Multiple peaks with a Gaussian distribution showing the presence of polyclonal T cells are seen in the spleen of mock-infected mice (control). The same pattern was found in the spleens of WNV-infected mice. In contrast, a single or a few peaks, signifying high levels of oligoclonality, were obtained from all VA and VB families tested in the WNV-infected brains.

levels of Th1-type cytokines and chemokines positively correlated with the propagation of WNV in the brains.

Infiltration of T cells in the brains of WNV-infected mice

To confirm the presence of brain-infiltrating T cells, expression of CD3, CD4, CD8, CD25, and CD69 was measured (Fig. 2*E*). CD3 and CD8 were expressed at low levels during the early phase of infection in WNV- and mock-infected brains. However, their expression considerably increased during the late phase of infection. CD25 and CD69 showed a similar expression pattern as CD3 and CD8. These results suggested that activated $CD3^+CD8^+$ T cells infiltrated the brains of the WNV-infected mice. CD4 transcripts were consistently detected in both WNV- and mock-infected mice. The expression of cytotoxic granule components (perforin, granzyme A, and granzyme B) was measured by qPCR (Fig. 2*F*) and found to be rapidly increased in the early stages of WNV infection in both spleens and brains, positively correlating with CD3, CD8, CD25, and CD69 expression. These results suggested that cytotoxic T lymphocytes expanded in the brains of WNV-infected mice.

TCR repertoire and clonality in brain-infiltrating T cells

TCRAV and TCRBV repertoires were analyzed from the spleens and brains of WNV- or mock-infected mice 10 d postinfection (Fig. 3*A*). The TCRAV and TCRBV repertoires were not significantly different in the spleens between the WNV- and the mock-infected mice. In contrast, the percentage frequencies of T cells bearing VA1-1, VA2-1, VB5-2, and VB8-2 were significantly higher in the brains of WNV-infected mice than in the spleens from WNV- or mock-infected mice. The expression levels of these families were increased from day 4 to day 10 in the brains (Fig. 4*A*). Expression of TCR genes was not detected in the brains from mock-infected mice. Furthermore, T cell clonality was examined by a CDR3 size spectratyping method and a significant increase in the clonality was detected in VA1-1, VA2-1, VB5-2, and VB8-2 (Fig. 3*B*). Polyclonal peak patterns were detected in the spleens of mock- and WNV-infected mice while oligoclonal or monoclonal peak patterns were detected in the brains of WNV-infected mice on day 10. Dominant peaks in VA1-1, VA2-1, and VB5-2 appeared to be identical in size among individual mice, whereas an oligoclonal peak pattern was detected in VB8-2.

Determination of CDR3 nucleotide sequences

CDR3 nucleotide sequences were determined with cDNA clones obtained from the spleen of mock-infected mice and the brains of WNV-infected mice. Predicted amino acid sequences with occurrence frequencies of the respective cDNA clones are shown in Fig 5. The cDNA clones obtained from the spleen of the mock-infected mice displayed highly diverse CDR3 sequences (data not shown), which corresponded to the results from CDR3 size spectratyping. In contrast, oligoclonal or monoclonal T cells were detected in VA1-1, VA2-1, and VB5-2 in the brains of WNV-infected mice.

In VA1-1, five clonotypes (CAVS-IG-NSGTYQRFG, CAVS-MG-NSGTYQRFG, CAVS-KG-NSGTYQRFG, CAVS-PG-NSGTYQRFG, and CAVS-MG-GYQNFYFG) were obtained from the brains of different mice (Fig. 5*A*). Interestingly, these clonotypes had only one amino acid difference in the N region. Additionally, preferential usage in AJ13 was observed in the WNV-infected brains (47 of 51 clones for mouse 1, 47 of 52 for mouse 2, 20 of 50 for mouse 3, 15 of 52 for mouse 4, and 25 of 51 for mouse 5). A similar result was also obtained from sequence analysis of VA2-1 (Fig. 5*B*). Two dominant clonotypes (CAAS-EG-GNYK-

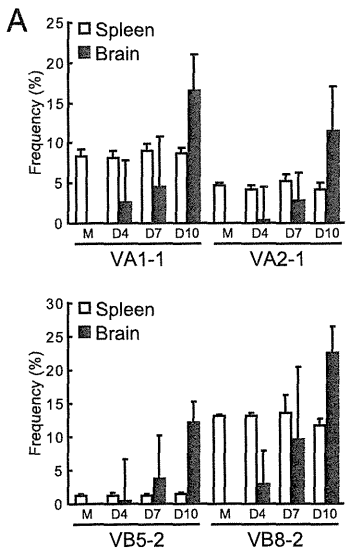

B

VA1-1

Day 4						Day 7					
Brain	Clonal frequency	V	N	J	J gene	Brain	Clonal frequency	V	N	J	J gene
#1	1/11	CA	AS I	SGSFNKLTFG	AJ04	#1	2/14	CAV	GTRA	QVVGQLTFG	AJ05
	1/11	CAV	MSS	TSGGNYKPTFG	AJ06		2/14	CAVS	MG	NSGTYQRFG	AJ13 ¶
	1/11	CAVS	R	NMGYKLTFG	AJ09		2/14	CA	VSAA	SSGQKLVFG	AJ16
	1/11	CA	VN	TNSAGNKLTFG	AJ17		2/14	CAV	LMS	TGSNRLTFG	AJ28
	1/11	CAAS		DRGSALGRLHFG	AJ18		1/14	CAVS	KG	NSGTYQRFG	AJ13 ⊖
	1/11	CA	ASM	PGTGSNRLTFG	AJ28		1/14	CAVS	ADG	QGGRALIFG	AJ15
	1/11	CAV	SK	NTRKLIFG	AJ37		1/14	CAV	HI	DRGSALGRLHFG	AJ18
	1/11	CAV	MT	NNAGAKLTFG	AJ39		1/14	CAV	AGG	TNTGKLTFG	AJ27
	1/11	CAAS	PA	SGGSNAKLTFG	AJ42		1/14	CAV	PA	FASALTFG	AJ35
	1/11	CAVS		GADRLTFG	AJ45		1/14	CAVS	PA	VGDNSKLIWG	AJ38
	1/11	CAVS	FSV	GGSNYKLTFG	AJ53	#2	2/12	CAVS	M	TNSAGNKLTFG	AJ17
#2	1/14	CA	VSIG	NTGGLSG	AJ02		2/12	CA	ATT	ASLGKLQFG	AJ24
	1/14	CA	VA	NSGTYQRFG	AJ13		2/12	CAAS	PP	NNYAQG	AJ26
	1/14	CAAS	D	QGGRALIFG	AJ15		1/12	CA	SALN	NTGYQNFYFG	AJ49
	1/14	CAA	F	GSALGRLHFG	AJ18		1/12	CAVS	MG	NSGTYQRFG	AJ13 ¶
	1/14	CAAS	ANL	NTNTGKLTFG	AJ27		1/12	CAVS	IG	NSGTYQRFG	AJ13 §
	1/14	CA	VR	PGTGSNRLTFG	AJ28		1/12	CAVS	VG	NSGTYQRFG	AJ13
	1/14	CAA	P	LPGTGSNRLTFG	AJ28		1/12	CAVS		SNTNKVVFG	AJ34
	1/14	CAVS	MAG	NNRIFFG	AJ31		1/12	CA	VL	SSSFSKLVFG	AJ50
	1/14	CA	VSL	GSSGNKLIFG	AJ32	#3	2/13	CAVS	RG	NSGTYQRFG	AJ13
	1/14	CA	VSH	SNYQLIWG	AJ33		2/13	CAV	M	RGSALGRLHFG	AJ18
	1/14	CA	VTL	NNAGAKLTFG	AJ39		2/13	CA	ASEA	GFASALTFG	AJ35
	1/14	CAV	RS	NTGYQNFYFG	AJ49		2/13	CAAS	GAS	GGSNAKLTFG	AJ42
	1/14	CAVS	KSM	SSFSKLVFG	AJ50		1/13	CAVS	KG	NSGTYQRFG	AJ13 ⊖
	1/14	CA	VRK	GGSAKLIFG	AJ57		1/13	CA	ASPL	TNTGKLTFG	AJ27
#3	1/12	CA	ASG	NMGYKLTFG	AJ09		1/13	CA	SLL	NTNKVVFG	AJ34
	1/12	CAV		NMGYKLTFG	AJ09		1/13	CAVS	TNT	NVGDNSKLIWG	AJ38
	1/12	CA	AG	SGTYQRFG	AJ13		1/13	CA	SGM	GADRLTFG	AJ45
	1/12	CA	VSIG	NNRIFFG	AJ31						
	1/12	CAA	RD	YGSSGNKLIFG	AJ32						
	1/12	CA	VSR	DSNYQLIWG	AJ33						
	1/12	CAAS	MK	GNTRKLIFG	AJ37						
	1/12	C	TVTH	NNAGAKLTSG	AJ39						
	1/12	CA	VS	NTEGADRLTFG	AJ45						
	1/12	CAAS	L	ASSSFSKLVFG	AJ50						
	1/12	CA	VSM	TGANTGKLTFG	AJ52						
	1/12	CAA	FH	QGGSAKLIFG	AJ57						

FIGURE 4. *A*, Increase in the percentage frequencies of T cells bearing VA1-1, VA2-1, VB5-2, and VB8-2 in WNV-infected mouse brains. *B*, Amino acid sequences of CDR3 regions of VA1-1 in WNV-infected mouse brains on day 4 and day 7 postinfection. Identical sequences detected in different individual mice are marked by the symbols.

A

VA 1-1

Brain	Clonal frequency	V	N	J	J gene	
#1	24/51	CAVS	IG	NSGTYQRFG	AJ13	§
	21/51	CAVS	MG	NSGTYQRFG	AJ13	¶
	3/51	CA	ASGL	SNTNKVVFG	AJ34	
	2/51	CAVS	KG	NSGTYQRFG	AJ13	Θ
	1/51	CA	AL	NTGYQNFYFG	AJ49	
#2	33/52	CAVS	LA	NSGTYQRFG	AJ13	
	8/52	CAVS	RG	NSGTYQRFG	AJ13	
	6/52	CAVS	MG	NSGTYQRFG	AJ13	¶
	3/52	CAVS	MG	GYQNFYFG	AJ49	†
	1/52	CA	ASME	GDNSKLIWG	AJ38	
	1/52	CA	AED	YANKMICG	AJ47	
#3	13/50	CAVS	PG	NSGTYQRFG	AJ13	‡
	9/50	CA	AN	NVGDNSKLIWG	AJ38	※
	8/50	CA	ASM	TGNTRKLIFG	AJ37	
	6/50	C	GGKEG	GADRLTFG	AJ45	
	4/50	CAVS	MG	NSGTYQRFG	AJ13	¶
	3/50	CAVS	MG	GYQNFYFG	AJ49	†
	3/50	CAVS	PA	NSGTYQRFG	AJ13	
	2/50	CAV		NTNTGKLTFG	AJ27	
	1/50	C	GGKG	GSALGRLHFG	AJ18	
	1/50	CA	ASI	NTNTGKLTFG	AJ27	
#4	26/52	CAV	RPT	ASLGKLQFG	AJ24	
	15/52	CAVS	IG	NSGTYQRFG	AJ13	§
	6/52	CAVS	RG	QGGRALIFG	AJ15	
	3/52	CAAS	P	SGGSNAKLTFG	AJ42	
	2/52	CA	ASEMD	YANKMICG	AJ47	
#5	18/51	CAVS	KG	NSGTYQRFG	AJ13	Θ
	12/51	CAVS		TNAYKVIFG	AJ30	
	9/51	CAVS	R	TQVVGQLTFG	AJ05	
	7/51	CAVS	PG	NSGTYQRFG	AJ13	‡
	4/51	CA	AN	NVGDNSKLIWG	AJ38	※
	1/51	CAV	LTG	GADRLTFG	AJ45	

B

VA 2-1

Brain	Clonal frequency	V	N	J	J gene	
#1	34/50	CAAS	EG	GNYKYVFG	AJ40	§
	6/50	CA	PRG	NNYAQGLTFG	AJ26	
	5/50	CAAS	EG	TNTGKLTFG	AJ27	
	3/50	CAA	VD	YANKMICGLG	AJ47	
	2/50	CAA		TGGNNKLTFG	AJ56	
#2	18/53	CAAS	G	GSALGRLHFG	AJ18	
	15/53	CAAS	VA	GNYKYVFG	AJ40	
	14/53	CAAS	EA	GNYKYVFG	AJ40	¶
	3/53	CAA	NEA	GNYKYVFG	AJ40	
	2/53	CAAS	AVY	NTNTGKLTFG	AJ27	
	1/53	CAAS	VS	SGGNYKPTFG	AJ06	
#3	15/52	CAA	RG	NNYAQGLTFG	AJ26	
	11/52	CAAS	EA	GNYKYVFG	AJ40	¶
	7/52	CAAS	G	NNYAQGLTFG	AJ26	
	6/52	CA	VRG	NNYAQGLTFG	AJ26	
	6/52	CAAS	EG	GNYKYVFG	AJ40	§
	5/52	CAAS	ET	GNYKYVFG	AJ40	
	2/52	CAA	RD	VGDNSKLIWG	AJ38	
#4	21/52	CAAS	EA	GNYKYVFG	AJ40	¶
	14/52	CAAS	P	TNAYKVIFG	AJ30	
	12/52	CAA	I	TGGNNKLTFG	AJ56	
	4/52	CAAS	MA	GNYKYVFG	AJ40	
	1/52	CA	G	NNNAGAKLTFG	AJ39	
#5	17/50	CAAS	EA	GNYKYVFG	AJ40	¶
	11/50	CAAS	LA	GNYKYVFG	AJ40	
	9/50	CAA	RGN	YAQGLTFG	AJ26	
	8/50	CAAS	NA	NAYKVIFG	AJ30	
	3/50	CAAS	AGD	NYAQGLTFG	AJ26	
	2/50	CA	V	NAGAKLTFG	AJ39	

C

VB 5-2

Brain	Clonal frequency	V	N-D-N	J	J gene
#1	49/52	CASS	PGTGG	YEQYFG	BJ2. 7
	3/52	CASS	RTG	SAETLYFG	BJ2. 3
#2	46/53	CASS	RGD	YAEQFFG	BJ2. 1
	5/53	CAS	FRGD	YAEQFFG	BJ2. 1
	2/53	CASS	GTGG	NERFFG	BJ1. 4
#3	34/51	CASS	LEL	YAEQFFG	BJ2. 1
	13/51	CASS	PEL	YAEQFFG	BJ2. 1
	4/51	CASS	LDP	EQYFG	BJ2. 7
#4	26/51	CASS	PRD	NYAEQFFG	BJ2. 1
	15/51	CASS	LGGG	SYEQYFG	BJ2. 7
	8/51	CASS	LLDN	AETLYFG	BJ2. 3
	2/51	CASS	LTGA	NTEVFFG	BJ1. 1
#5	42/51	CASS	LRDS	YAEQFFG	BJ2. 1
	9/51	CASS	LNRV	YAEQFFG	BJ2. 1

D

VB 8-2

Brain	Clonal frequency	V	N	J	J gene
#1	18/52	CASG	DWGGAQ	SQNTLYFG	BJ2. 4
	10/52	CASG	DRTGL	NERLFFG	BJ1. 4
	9/52	CASG	DWTGK	SQNTLYFG	BJ2. 4
	7/52	CASG	EWGG	AEQFFG	BJ2. 1
	3/52	CASG	DVGQG	NTEVFFG	BJ1. 1
	3/52	CAS	SATTGG	NSDYTFG	BJ1. 2
	2/52	CASG	DDR	YEQYFG	BJ2. 7
#2	28/53	CASG	DWAGFS	SYEQYFG	BJ2. 7
	9/53	CAS	SDDRG	SAETLYFG	BJ2. 3
	9/53	CASG	DPGG	SYEQYFG	BJ2. 7
	3/53	CASG	ESGARD	NSPLYFA	BJ1. 6
	2/53	CAS	SPGTP	SYEQYFG	BJ2. 7
	1/53	CAS	SDGTGDN	NSPLYFA	BJ1. 6
	1/53	CASG	ERAGFS	SYEQYFG	BJ2. 7
#3	16/50	CASG	DWG	DTQYFG	BJ2. 5
	13/50	CASG	DAG	NQDTQYFG	BJ2. 5
	8/50	CASG	DAWGR	EQYFG	BJ2. 7
	7/50	CASG	DWTGDT	YAEQFFG	BJ2. 1
	3/50	CASG	DGGG	EQYFG	BJ2. 7
	2/50	CASG	DWTGGAG	QNTLYFG	BJ2. 4
	1/50	CASG	DWTGD	NYAEQFFG	BJ2. 1
#4	32/51	CASG	GLGS	SAETLYFG	BJ2. 3
	8/51	CASG	DWTGGD	ERLFFG	BJ1. 4
	5/51	CASG	DAGN	SYEQYFG	BJ2. 7
	4/51	CASG	DWTGGALG	QNTLYFG	BJ2. 4
	2/51	CASG	DL	YNSPLYFAAG	BJ1. 6
#5	16/50	CASG	GTGGL	NTLYFG	BJ2. 4
	13/50	CASG	EPGGA	NTLYFG	BJ2. 4
	8/50	CASG	DARD	SNERFFG	BJ1. 4
	4/50	CAS	RPRDWGN	YEQYFG	BJ2. 7
	3/50	CASG	DARTN	SGNTLYFG	BJ1. 3
	3/50	CAS	SDWGA	SAETLYFG	BJ2. 3
	2/50	CASG	AQGG	ETLYFG	BJ2. 3
	1/50	CASG	DEE	NTLYFG	BJ2. 4

FIGURE 5. Amino acid sequences of CDR3 regions of VA1-1 (*A*), VA2-1 (*B*), VB5-2 (*C*), and VB8-2 (*D*) in WNV-infected mice brain on day 10. In each family, identical sequences detected in different individual mice are marked by the symbols.

YVFG and CAAS-EA-GNYKYVFG) appeared from the brains of different mice. These clonotypes had similar CDR3 sequences and the common AJ40 segment. Sequence analysis with VB5-2 exhibited extremely high levels of oligoclonality: 49 of 52 clones in mouse 1, 46 of 53 clones in mouse 2, 34 of 51 clones in mouse 3, 26 of 51 clones in mouse 4, and 42 of 51 clones in mouse 5 had identical CDR3 sequences (Fig. 5*C*). However, these dominant VB5-2 clonotypes were different among the brains of mice. Similarly, dominant clonotypes obtained from VB8-2 had different CDR3 sequences among individual mice (Fig. 5*D*). These results indicated that oligoclonal T cells expanded in the brains of mice in response to WNV infection, and that the brain-infiltrating T cells used a highly restricted and shared TCRAV repertoire, but a somewhat diverse TCRBV repertoire.

To clarify T cell clonalities at an early time point during infection, we performed CDR3 sequence analyses using samples obtained from the brains on days 4 and 7 (Fig. 4). Brain T cells showed a more diverse TCR repertoire on days 4 and 7 compared with those on day 10 (Fig. 4*B*). On day 7, T cells showed some degree of oligclonality, and interestingly, several clonotypes (CAVS-MG-NSGTYQRFG, CAVS-KG-NSGTYQRFG, and CAVS-IG-NSGTYQRFG) that presented dominantly on day 10 were obtained at low frequency on day 7 (Fig. 4*B*). These results suggest that oligoclonal T cells are generated by local expansion within the brains, not migration from the periphery.

Comparison of the TCR repertoire among closely related flaviviruses

TCR repertoires were also analyzed with spleens and brains from mice infected with closely related flaviviruses, JEV and TBEV (Fig. 6). The percentage frequencies of T cells bearing VA1-1, VA3-1, and VB9-1 were significantly higher in the brains of TBEV-infected mice than in the spleens from mock-infected mice. We have previously reported that the percentage frequencies of T cells bearing VA5-1, VA17-1, VA19-1, VB2-1, VB8-3, and VB13-1 were significantly increased in the brains of JEV-infected mice (7). These results demonstrated that TCR repertoires used by the brain-infiltrating T lymphocytes were different among WNV-,

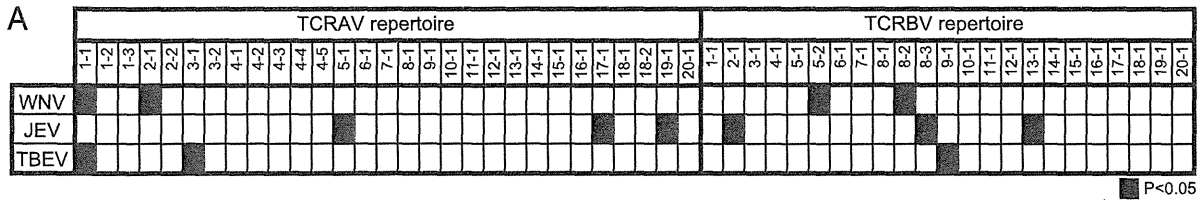

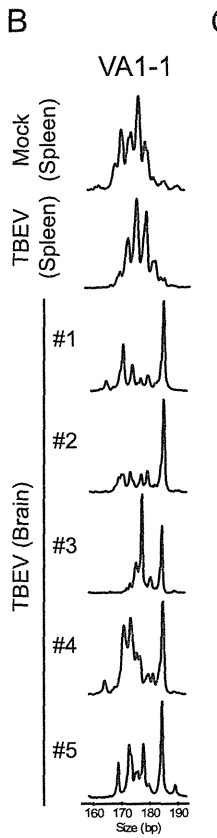

C

VA1-1

Brain	Clonal frequency	V	N	J	J gene	
#1	11/52	CAAS	ERG	YGGSGNKLIFG	AJ32	§
	8/52	CAAS	ERD	YGGSGNKLIFG	AJ32	¶
	6/52	CA	V	DSGYNKLTFG	AJ11	
	6/52	CA	VD	NTNTGKLTFGDG	AJ27	
	5/52	CAAS	ERY	YGGSGNKLIFG	AJ32	Θ
	5/52	CAAS	ERF	YGGSGNKLIFG	AJ32	†
	2/52	CAAS	ERS	YGGSGNKLIFG	AJ32	‡
	1/52	CA	VF	MGYKLTFG	AJ09	
	1/52	CA	VSM	MGYKLTFG	AJ09	
	1/52	CAAS	VH	NNRIFFG	AJ31	
	1/52	CAAS	ERT	YGGSGNKLIFG	AJ32	ж
	1/52	CAAS	ERR	YGGSGNKLIFG	AJ32	
	1/52	CA	VSG	GGSGNKLIFG	AJ32	
	1/52	CA	V	SNYQLIWGSG	AJ33	
	1/52	CAA	F	NTGNYKYVFG	AJ40	
	1/52	CA	G	NNNNAPRFG	AJ43	
#2	14/51	CAAS	ERG	YGGSGNKLIFG	AJ32	§
	9/51	CAAS	ERN	YGGSGNKLIFG	AJ32	@
	6/51	CAA		DTNAYKVIFG	AJ30	
	4/51	CAAS	ERI	YGGSGNKLIFG	AJ32	Й
	4/51	CAAS	ERE	YGGSGNKLIFG	AJ32	
	3/51	CAAS	ERY	YGGSGNKLIFG	AJ32	Θ
	2/51	CAAS	ERD	YGGSGNKLIFG	AJ32	¶
	2/51	CAAS	ERA	YGGSGNKLIFG	AJ32	
	2/51	CAAS	ERP	YGGSGNKLIFG	AJ32	
	1/51	CAA	RG	QGGRALIFG	AJ15	
	1/51	CAAS	DP	NAYKVIFG	AJ30	
	1/51	CAAS	ERT	YGGSGNKLIFG	AJ32	ж
	1/51	CAA	REG	SSNTNKVVFG	AJ34	
	1/51	CA	V	NNNNAPRFG	AJ43	
#3	30/50	CAAS	IGD	MGYKLTFG	AJ09	
	5/50	CAAS	ERG	YGGSGNKLIFG	AJ32	§
	3/50	CAAS	EQN	YGGSGNKLIFG	AJ32	
	3/50	CAAS	ERN	YGGSGNKLIFG	AJ32	@
	2/50	CAAS	ERV	YGGSGNKLIFG	AJ32	
	2/50	CAAS	ERD	YGGSGNKLIFG	AJ32	¶
	1/50	CAAS	EQV	YGGSGNKLIFG	AJ32	
	1/50	CAAS	ERGW	GGSGNKLIFG	AJ32	
	1/50	CAA	H	YGSSGNKLIFG	AJ32	
	1/50	CAAS	GA	NTNKVVFG	AJ34	
	1/50	CA	ES	NNNNAPRFG	AJ43	

Brain	Clonal frequency	V	N	J	J gene	
#4	12/53	CAAS	ERN	YGGSGNKLIFG	AJ32	@
	9/53	CAAS	ERS	YGGSGNKLIFG	AJ32	‡
	6/53	CAAS	ERG	YGGSGNKLIFG	AJ32	§
	6/53	CAAS	G	GGRALIFG	AJ15	
	5/53	CAAS	ERI	YGGSGNKLIFG	AJ32	Й
	2/53	CAAS	P	GGRALIFG	AJ15	
	2/53	CAA	IP	NYNVLYFG	AJ21	
	2/53	CAAS	W	NRIFFG	AJ31	
	1/53	CA	PP	NSAGNKLTFG	AJ17	
	1/53	CA	RT	NSAGNKLTFG	AJ17	
	1/53	CAAS	EGHT	ASLGKLQFG	AJ24	
	1/53	CA	V	DTNAYKVIFG	AJ30	д
	1/53	CAAS	ERSH	GGSGNKLIFG	AJ32	
	1/53	CAAS		NTGNYKYVFG	AJ40	
	1/53	CAAS	LDTG	GADRLTFG	AJ45	
	1/53	CAAS	EHD	YGNEKITFG	AJ48	
	1/53	CAAS	EGG	NYGNEKITFG	AJ48	
#5	11/52	CAAS	ERG	YGSSGNKLIFG	AJ32	§
	8/52	CA	G	NNAGAKLTFG	AJ39	
	7/52	CAAS	ERN	YGSSGNKLIFG	AJ32	@
	6/52	CAAS	E	GFASALTFG	AJ35	
	5/52	CA	V	DTNAYKVIFG	AJ30	д
	5/52	CAAS	EQR	YGSSGNKLIFG	AJ32	
	3/52	CA	V	NYAQG	AJ26	
	2/52	CAAS	ERF	YGSSGNKLIFG	AJ32	†
	1/52	CAAS	KA	GGYKVVFG	AJ12	
	1/52	CA	V	TGGYKVVFG	AJ12	
	1/52	CA	VMP	NYNVLYFG	AJ21	
	1/52	CAAS	N	GFASALTFG	AJ35	
	1/52	CA	VS	TGNTGKLIFG	AJ37	

FIGURE 6. Comparison of TCR repertoires of brain-infiltrating T lymphocytes among WNV-, JEV-, and TBEV-infected mice. *A*, TCRAV and TCRBV repertoires, which were increased in the brains by infection with WNV, JEV, or TBEV, are indicated by filled boxes ($p < 0.05$, Student unpaired t test, $n = 5$). TCR repertoire of T cells in JEV-infected mouse brains was reported previously (7). *B*, CDR3 size spectratyping of T cells bearing VA1-1 in TBEV-infected mouse brains. *C*, Amino acid sequences of CDR3 regions of VA1-1 in TBEV-infected mouse brains. Identical sequences detected in different individual mice are marked by the symbols.

TBEV-, and JEV-infected mice, with the exception of VA1-1, which increased significantly in WNV as well as TBEV (Fig. 6*A*). T cell clonality was examined in TBEV-infected mice brain, with a VA1-1–specifc primer by CDR3 size spectratyping (Fig. 6*B*). Oligoclonal peak patterns of T cells were detected in all five TBEV-infected mice. A dominant peak was identical in length among five mice. However, the length of the dominant peak was different between WNV- and TBEV-infected mice brain (Figs. 3*B*, 6*B*).

To examine whether these expanding T cells shared identical or similar TCR repertoires between WNV- and TBEV-infected mice, the nucleotide sequences of CDR3 were determined for VA1-1 cDNA clones from TBEV-infected mice (Fig. 6*C*). Nine clonotypes (CAAS-ERX-YGGSGNKLIFG; X of N region including G, D, Y, F, S, T, N, and I; and CA-V-DTNAYKVIFG) were detected in different mice. These clonotypes had highly similar CDR3 sequences and differed in a single amino acid residue within the N region. Additionally, preferential usage of AJ32 was observed in VA1-1 of the TBEV-infected brains. However, there was no similarity in CDR3 sequences between clonotypes obtained from WNV-infected and TBEV-infected mice. These results indicated that the brain-infiltrating T cells induced by closely related viruses, namely WNV, JEV, and TBEV, did not use shared TCR repertoires.

Cross-reaction of brain-infiltrating T cells between WNV and JEV in vitro

The specificity and cross-reactivity of brain-infiltrating T cells were examined. T cells isolated from either WNV- or JEV-infected C3H/HeN (H-2k) mouse brains were cultured for 12 h with PECs infected with WNV or JEV. Levels of IFN-γ and TNF-α were assessed by ELISA in the culture supernatant fluids (Table II). High levels of IFN-γ and TNF-α were detected in the supernatants of T cells from WNV-infected mouse brains after stimulation with WNV-infected PECs of C3H/HeN mice, but not after stimulation with JEV-infected PECs of C3H/HeN mice or WNV-infected PECs from mice with different MHC haplotypes. High IFN-γ and TNF-α production was also detected in the supernatants of T cells from JEV-infected mouse brains only after stimulation with JEV-infected PECs of C3H/HeN mice. Additionally, in vitro stimulation of $CD4^+$ or $CD8^+$ cells isolated separately from WNV-infected mouse brain was performed (Table III). The results

Table II. IFN-γ and TNF-α production by T cells isolated from WNV- or JEV-infected C3H/HeN mouse brains after in vitro stimulation with WNV or JEV

PECs Isolated from	Virus Infection	IFN-γ Production (pg/ml)		TNF-α Production (pg/ml)	
		T Cells Isolated from WNV-Infected C3H/HeN Mice Brain	T Cells Isolated from JEV-Infected C3H/HeN Mice Brain	T Cells Isolated from WNV-Infected C3H/HeN Mice Brain	T Cells Isolated from JEV-Infected C3H/HeN Mice Brain
C3H/HeNJcl (H-2^k)	WNV	1446.6 ± 55.5	20.3 ± 8.5	476.9 ± 46.7	26.4 ± 9.8
	JEV	18.7 ± 3.1	1038.2 ± 53.4	19.8 ± 7.2	370.1 ± 84.1
	None	18.3 ± 4.5	17.5 ± 6.5	22.7 ± 3.1	25.2 ± 4.9
C57BL/6JJcl (H-2^b)	WNV	24.1 ± 7.2	22.1 ± 4.4	21.9 ± 6.1	25.3 ± 7.4
	JEV	26.3 ± 8.6	24.7 ± 3.9	19.2 ± 4.3	24.2 ± 5.4
	None	25.0 ± 6.5	20.1 ± 4.2	23.3 ± 5.9	26.2 ± 6.2
BALB/cAJcl (H-2^d)	WNV	15.7 ± 2.5	21.1 ± 7.1	27.2 ± 8.4	24.1 ± 4.7
	JEV	18.9 ± 3.6	23.7 ± 5.8	26.3 ± 6.0	24.4 ± 1.2
	None	23.3 ± 7.5	24.7 ± 2.2	27.0 ± 9.1	29.6 ± 3.3

Levels of IFN-γ and TNF-α were assessed by ELISA in the supernatants of T cells isolated from WNV- or JEV-infected mouse brains (n = 8) after in vitro stimulation for 12 h with PECs infected with WNV or JEV. Numbers indicate the mean ± SD of IFN-γ and TNF-α production (pg/ml) in triplicate wells.

indicate that $CD8^+$ cells isolated from the brains of mice infected with WNV were virus-specific, but not cross-reactive, between WNV and JEV, and that $CD4^+$ T cells were not WNV-specific.

T cells from WNV-infected mouse brains were cultured with PECs infected with WNV for 3 d. CDR3 sequences of VA1-1 and VA2-1 were compared before and after in vitro stimulation (Table IV). Before stimulation, the pooled T cells exhibited oligoclonality with several TCR clonotypes that were identical to the dominant TCR clonotypes found in five individual mice in Fig. 5. After stimulation for 3 d, the T cells also showed extensive clonality for both VA1-1 and VA2-1 (Table IV). The dominant CDR3 sequences were maintained after stimulation, suggesting the expansion of specific T cell clones.

Discussion

WNV (strain NY99-6922) induced encephalitis in C3H/HeN mice after i.p. administration. Histopathological analysis demonstrated encephalitic changes, CNS degeneration, and infiltration of $CD3^+$ $CD8^+$ T cells in the brains of WNV-infected mice. This corresponds to the fact that the expression level of CD3 and CD8 positively correlated with viral RNA levels in the brains of WNV-infected mice. These results suggest that $CD8^+$ T cells predominantly infiltrated in the brains as infection progressed. It has been reported that tissue destruction and the presence of $CD3^+$ $CD8^+$ T cells were found in the brains of JEV- and TBEV-infected mice (7, 24). There are reports on human T cell responses following in vitro stimulation of PBMCs from WNV-infected patients with peptides derived from WNV Ags (25, 26). They indicated a critical role of $CD8^+$ T cells and IFN-γ production in responses to a limited number of epitopes with MHC restriction. The similar nature of T cell immunity between humans and mice supports the idea that the murine model in the present study is useful for elucidating the characteristics of brain-infiltrating T cells during flavivirus infection. This will lead to greater understanding of T cell immune responses in WNV-infected humans.

$CD4^+$ cells were stained and their transcripts were persistently expressed at a high level in both mock and infected mouse brains. This is probably due to the presence of microglia that express CD4 in CNS resident cells (27, 28). These results do not necessarily mean that $CD4^+$ T cells are absent in the WNV-infected brains. It has been reported that both $CD4^+$ and $CD8^+$ T cells increase in the brains after WNV infection (29). The CD4 transcripts expressed by the microglia, which are abundantly present in the CNS, might mask more $CD4^+$ T cells in the brains. Notably, the expression level of the contents of cytotoxic granules, such as perforin, granzyme A, and granzyme B, were positively related to the increase in CD8 in the brain. These cytotoxicity-related genes were mainly expressed in activated $CD8^+$ cells or NK cells, but not in $CD4^+$ cells. It is known that $CD8^+$ T cells are activated separately from NK cells in WNV-infected mouse brains (30). These results suggest that most of the brain-infiltrating T lymphocytes are cytotoxic $CD8^+$ T cells.

Th1-type cytokines were largely induced in the brains in response to WNV infection. The increased expression of IFN-γ, TNF-α, and IL-2 were remarkable on day 10 after viral infection, suggesting that Th1 cytokine-producing T cells contribute to antiviral response in the CNS. It is of interest that IL-10 was abundantly expressed in both the spleens and brains. A recent report demonstrated that IL-10 was mainly produced by $CD4^+$ cells and was dramatically elevated in WNV-infected mice (31). Given that IL-10 controls host immune responses by suppressing Th1 responses (32), elevated production of IL-10 impacts on WNV

Table III. IFN-γ and TNF-α production by $CD8^+$ cells, but not $CD4^+$ cells, isolated from WNV-infected C3H/HeN mouse brains after in vitro stimulation with WNV- or JEV-infected PECs in C3H/HeN mice

C3H/HeN PECs Infected with	Isolated Cells from WNV-Infected C3H/HeN Mice Brain			
	IFN-γ Production (pg/ml)		TNF-α Production (pg/ml)	
	$CD4^+$ Cells	$CD8^+$ Cells	$CD4^+$ Cells	$CD8^+$ Cells
WNV	15.4 ± 4.2	1358.1 ± 74.5	26.4 ± 3.9	623.6 ± 49.2
JEV	17.1 ± 4.7	19.8 ± 8.2	23.9 ± 5.8	23.1 ± 6.1
None	16.6 ± 6.1	24.7 ± 6.9	24.1 ± 7.7	28.5 ± 2.7

Levels of IFN-γ and TNF-α were assessed by ELISA in supernatants of $CD4^+$ or $CD8^+$ cells isolated from WNV-infected mouse brains (n = 8) after in vitro stimulation for 12 h with PECs infected with WNV or JEV. Numbers indicate the mean ± SD of IFN-γ and TNF-α production (pg/ml) in three wells.

Table IV. T cell clonalities in WNV-infected mouse brains before and after in vitro stimulation with PECs infected with WNV

Clonal Frequency	V	N	J	J Gene[a]	Frequency[b]
VA1-1 (prestimulation)					
12/55	CAVS	IG	NSGTYQRFG	AJ13 #	2/5
10/55	CAVS	LA	NSGTYQRFG	AJ13 $	1/5
8/55	CAVS	MG	NSGTYQRFG	AJ13 §	3/5
7/55	CAVS	KG	NSGTYQRFG	AJ13 †	2/5
6/55	CAV	RPT	ASLGKLQFG	AJ24 ‡	1/5
4/55	CAVS	PG	NSGTYQRFG	AJ13	2/5
4/55	CAVS		TNAYKVIFG	AJ30	0/5
2/55	CAVS	RG	NSGTYQRFG	AJ13	1/5
1/55	CAVS	RG	QGGRALIFG	AJ15	1/5
1/55	CAVS	MG	GYQNFYFG	AJ49	2/5
VA1-1 (poststimulation)[d]					
37/52	CAVS	IG	NSGTYQRFG	AJ13 #	2/5
10/52	CAVS	MG	NSGTYQRFG	AJ13 §	3/5
3/52	CAVS	KG	NSGTYQRFG	AJ13 †	2/5
1/52	CAVS	LA	NSGTYQRFG	AJ13 $	1/5
1/52	CAV	RPT	ASLGKLQFG	AJ24 ‡	1/5
VA2-1 (prestimulation)[c]					
14/51	CAAS	EA	GNYKYVFG	AJ40 #	4/5
11/51	CAAS	EG	GNYKYVFG	AJ40 $	2/5
7/51	CAAS	G	GSALGRLHFG	AJ18	1/5
6/51	CAA	RG	NNYAQGLTFG	AJ26 §	1/5
4/51	CAAS	VA	GNYKYVFG	AJ40 †	1/5
3/51	CAAS	G	NNYAQGLTFG	AJ26	1/5
2/51	CAAS	NA	NAYKVIFG	AJ30	1/5
2/51	CAA	I	TGGNNKLTFG	AJ56	1/5
1/51	CA	PRG	NNYAQGLTFG	AJ26	1/5
1/51	CAAS	P	TNAYKVIFG	AJ30	1/5
VA2-1 (poststimulation)[d]					
35/54	CAAS	EG	GNYKYVFG	AJ40 $	2/5
16/54	CAAS	EA	GNYKYVFG	AJ40 #	4/5
2/54	CAA	RG	NNYAQGLTFG	AJ26 §	1/5
1/54	CAAS	VA	GNYKYVFG	AJ40 †	1/5

[a]Identical sequences observed in both pre- and poststimulation are marked by respective symbols in the column.
[b]The frequency indicates the number of mice, among a total of five, where the clones with the respective CDR3 sequences were detected in Fig. 5.
[c]T cells were isolated from eight WNV-infected C3H/HeN mouse brains and pooled ($n = 8$). CDR3 regions of cDNA clones containing VA1-1 and VA2-1 were sequenced.
[d]T cells were stimulated in vitro with PECs infected with WNV at 37°C for 3 d and were subjected to CDR3 sequence analysis.

pathogenesis by preventing the host from inducing a hyperinflammatory immune reaction. It is known that chemokines and chemokine receptors are important to the pathogenesis of WNV infection. Microglia and astrocytes secrete the chemokines CCL5 and CXCL10 (33), which recruit effector T cells via the chemokine receptors CXCR3 (19, 34) and CCR5 (29) in C57BL/6J mice, respectively. The expression levels of the chemokines CCL5 and CXCL10 increased >100-fold in the brains, whereas the increases in their receptors, CCR5 and CXCR3, were not as pronounced in C3H mice. As has been previously reported (35), the expression levels of early (CD25) and late (CD69) T cell activation markers were increased with time. Thus, it is likely that the brain-infiltrating T lymphocytes are mostly supplied by local expansion of $CD8^+$ T cells, rather than by the recruitment of $CCR5^+$ or $CXCR3^+$ T cells across the blood–brain barrier by the CCL5 and CXCL10.

TCR mRNA was below detectable levels in the mock brains because of poor infiltration of T cells. In contrast, TCR expression was ~100-fold higher in WNV-infected brains on day 10 compared with mock-infected brains. There is a possibility that the accumulation of T cells in the brains is caused by nonspecific migration from peripheral organs and random leakage from peripheral blood. However, the T cells showed high oligoclonality in their TCR repertoires that were completely different between WNV-infected mice and JEV-infected mice. Moreover, a few T cells that resided within the brains increased drastically from day 7 to day 10. These results suggest that the increase in the number of $CD8^+$ T cells in the brains is mainly due to local expansion of T cells that recognize different Ags among closely related viruses.

TCR usage was found to be completely different between WNV- and JEV-infected mice brains; this is not, however, consistent with cross-reactivity of Abs between WNV and JEV (15). MHC-restricted cytotoxic T cells against WNV-infected target cells were detected in mice (36, 37), and mouse spleen cells immunized with JEV partially lysed WNV-infected target cells (38, 39). Peptide variants derived from 9-aa residues of NS4b elicit cross-reactive $CD8^+$ T cells in both JEV and WNV, whereas their functional and phenotypic properties were different between JEV and WNV (40). In our studies, the brain-infiltrating $CD8^+$ T cells showed a similar characteristic, namely a Th1/Tc1 phenotype, between WNV- and JEV-infected mice. $CD8^+$ T cells isolated from virus-infected mouse brains produced IFN-γ and TNF-α after coculture in vitro with virus-infected PECs with syngeneic

MHC haplotype, suggesting that the $CD8^+$ T cells within brains are virus-specific and not cross-reactive with other flaviviruses. Moreover, dominant T cells with a high clonality were detected in the brains of different individual mice, suggesting that they were not induced by bystander activation of nonspecific T cells. These results strongly suggest that the dominant T cells elicited in brains by in vivo primary WNV infection are virus-specific and not crossreactive. It is possible that the cross-reactive T cells are subdominant in the brain following primary WNV infection. Cellular cloning techniques or sequential stimulation in vitro with Ag probably induce a skewed hierarchy of T cells and may not be genuinely representative of the in vivo T cell populations. The direct cloning of TCR genes from local inflammatory sites would be a powerful tool for understanding T cell-mediated immunopathology and recovery in WNV encephalitis.

CDR3 sequence analysis revealed interesting results on Ag specificity. Most TCR clonotypes obtained from the brains of flavivirus-infected mice showed preferential usage of AJ segments (AJ13 for VA1-1 of WNV, AJ40 for VA2-1 of WNV, AJ32 for VA1-1 of TBEV). For WNV-infected mice, TCR clonotypes derived from VA1-1 contained rich hydrophobic amino acids such as alanine, glycine, isoleucine, leucine, methionine, and proline in the N region (126 of 154 residues). TBEV-infected mice frequently used an ERX motif (for glutamate, arginine, and X, which represents any amino acid), which contains polar amino acids in the N region. The dissimilarity in CDR3α sequences suggests the expansion of T cells with different Ag specificities between WNV-infected mice and TBEV-infected mice. The brain-infiltrating T lymphocytes did not share identical TCR repertoires between WNV-infected and JEV-infected mice (7).

In contrast to the very restricted TCRAV repertoire, the brain-infiltrating T lymphocytes exhibited relatively broad TCRBV repertoires. In VB5-2, CDR3 sequences varied considerably among individual mice, although BJ usage was limited to BJ2.1 and BJ2.7. Similarly, a common CDR3 sequence was not found in VB8-2 among individual mice. This contrasting result probably reflects a different role of TCR α- and β-chains in Ag recognition. The difference in the extent of repertoire restriction between TCR α- and β-chains has been shown in mice infected with JEV, a closely related flavivirus (7). Usage of restricted TCRAV and broad TCRBV has been reported in infection with other viruses, such as herpesvirus (41). Moreover, several reports have also described a dominant and essential role of the TCR α-chain in Ag recognition by T cells (42–44). It has been reported that TCRαβ heterodimers bearing a restricted TCR α-chain and diverse TCR β-chains have the potential to specifically recognize a single Ag in vitro (45). The dominant role of TCR α-chain is reflected to the restriction of the TCR β-chain repertoire observed in the brain-infiltrating T lymphocytes of WNV-infected mice.

We defined day 10 as the humane endpoint because this WNV-infected encephalitis mouse model was produced by administration of a lethal dose of the virus. Therefore, we could not observe $CD8^+$ T cell immune responses at later time points in animals that had recovered or not. It is known that the mortality rate is higher in CD8KO mice than in control mice and that $CD8^+$ T cells within the brain could play a protective role in the hosts (5). We recently reported that T cells that migrated into the brain following administration of a low dose of TBEV were different between living and dying mice (46). Further studies are needed to clarify the protective or immunopathological role of $CD8^+$ T cells by using low-dose administration of WNV.

In conclusion, Th1-like cytotoxic $CD8^+$ T cells with high clonality infiltrate into the brains of WNV-infected mice. These oligoclonal brain-infiltrating T cells use unique TCR repertoires, which are generated by a limited TCRα and diverse TCRβ genes. Moreover, the dominant brain-infiltrating $CD8^+$ T cells elicited in vivo by primary WNV infection are virus-specific, but not cross-reactive, among related flaviviruses. The present study provides important information on Ag specificity and diversity of WNV-specific $CD8^+$ T cells, as well as a new insight into the critical role of brain-infiltrating T cells in the recovery from WNV infection.

Acknowledgments

We thank Hiro Yamada and Tokikazu Nagaoka (Clinical Research Center, National Sagamihara Hospital) for assistance with our assay. We also thank Dr. Soichi Nukuzuma (Kobe Institute of Health, Kobe, Hyogo, Japan) for supplying a standard density of in vitro-synthesized WN virus NY99 RNA.

Disclosures

The authors have no financial conflicts of interest.

References

1. Petersen, L. R., and A. A. Marfin. 2002. West Nile virus: a primer for the clinician. *Ann. Intern. Med.* 137: 173–179.
2. Petersen, L. R., and J. T. Roehrig. 2001. West Nile virus: a reemerging global pathogen. *Emerg. Infect. Dis.* 7: 611–614.
3. Watson, J. T., P. E. Pertel, R. C. Jones, A. M. Siston, W. S. Paul, C. C. Austin, and S. I. Gerber. 2004. Clinical characteristics and functional outcomes of West Nile fever. *Ann. Intern. Med.* 141: 360–365.
4. Dauphin, G., S. Zientara, H. Zeller, and B. Murgue. 2004. West Nile: worldwide current situation in animals and humans. *Comp. Immunol. Microbiol. Infect. Dis.* 27: 343–355.
5. Shrestha, B., and M. S. Diamond. 2004. Role of $CD8^+$ T cells in control of West Nile virus infection. *J. Virol.* 78: 8312–8321.
6. Purtha, W. E., N. Myers, V. Mitaksov, E. Sitati, J. Connolly, D. H. Fremont, T. H. Hansen, and M. S. Diamond. 2007. Antigen-specific cytotoxic T lymphocytes protect against lethal West Nile virus encephalitis. *Eur. J. Immunol.* 37: 1845–1854.
7. Fujii, Y., K. Kitaura, K. Nakamichi, T. Takasaki, R. Suzuki, and I. Kurane. 2008. Accumulation of T-cells with selected T-cell receptors in the brains of Japanese encephalitis virus-infected mice. *Jpn. J. Infect. Dis.* 61: 40–48.
8. Davis, M. M. 1990. T cell receptor gene diversity and selection. *Annu. Rev. Biochem.* 59: 475–496.
9. Ding, Y. H., K. J. Smith, D. N. Garboczi, U. Utz, W. E. Biddison, and D. C. Wiley. 1998. Two human T cell receptors bind in a similar diagonal mode to the HLA-A2/Tax peptide complex using different TCR amino acids. *Immunity* 8: 403–411.
10. Gotoh, A., Y. Hamada, N. Shiobara, K. Kumagai, K. Seto, T. Horikawa, and R. Suzuki. 2008. Skew in T cell receptor usage with polyclonal expansion in lesions of oral lichen planus without hepatitis C virus infection. *Clin. Exp. Immunol.* 154: 192–201.
11. Matsutani, T., K. Shiiba, T. Yoshioka, Y. Tsuruta, R. Suzuki, T. Ochi, T. Itoh, H. Musha, T. Mizoi, and I. Sasaki. 2004. Evidence for existence of oligoclonal tumor-infiltrating lymphocytes and predominant production of T helper 1/T cytotoxic 1 type cytokines in gastric and colorectal tumors. *Int. J. Oncol.* 25: 133–141.
12. Shiobara, N., Y. Suzuki, H. Aoki, A. Gotoh, Y. Fujii, Y. Hamada, S. Suzuki, N. Fukui, I. Kurane, T. Itoh, and R. Suzuki. 2007. Bacterial superantigens and T cell receptor β-chain-bearing T cells in the immunopathogenesis of ulcerative colitis. *Clin. Exp. Immunol.* 150: 13–21.
13. Kitaura, K., K. Kanayama, Y. Fujii, N. Shiobara, K. Tanaka, I. Kurane, S. Suzuki, T. Itoh, and R. Suzuki. 2009. T cell receptor repertoire in BALB/c mice varies according to tissue type, sex, age, and hydrocortisone treatment. *Exp. Anim.* 58: 159–168.
14. Matsutani, T., T. Ohmori, M. Ogata, H. Soga, T. Yoshioka, R. Suzuki, and T. Itoh. 2006. Alteration of T-cell receptor repertoires during thymic T-cell development. *Scand. J. Immunol.* 64: 53–60.
15. Lim, C. K., T. Takasaki, A. Kotaki, and I. Kurane. 2008. Vero cell-derived inactivated West Nile (WN) vaccine induces protective immunity against lethal WN virus infection in mice and shows a facilitated neutralizing antibody response in mice previously immunized with Japanese encephalitis vaccine. *Virology* 374: 60–70.
16. Takashima, I., K. Morita, M. Chiba, D. Hayasaka, T. Sato, C. Takezawa, A. Igarashi, H. Kariwa, K. Yoshimatsu, J. Arikawa, and N. Hashimoto. 1997. A case of tick-borne encephalitis in Japan and isolation of the the virus. *J. Clin. Microbiol.* 35: 1943–1947.
17. Hayasaka, D., L. Ivanov, G. N. Leonova, A. Goto, K. Yoshii, T. Mizutani, H. Kariwa, and I. Takashima. 2001. Distribution and characterization of tick-borne encephalitis viruses from Siberia and far-eastern Asia. *J. Gen. Virol.* 82: 1319–1328.
18. Kasahara, T., T. Miyazaki, H. Nitta, A. Ono, T. Miyagishima, T. Nagao, and T. Urushidani. 2006. Evaluation of methods for duration of preservation of RNA quality in rat liver used for transcriptome analysis. *J. Toxicol. Sci.* 31: 509–519.

19. Klein, R. S., E. Lin, B. Zhang, A. D. Luster, J. Tollett, M. A. Samuel, M. Engle, and M. S. Diamond. 2005. Neuronal CXCL10 directs $CD8^+$ T-cell recruitment and control of West Nile virus encephalitis. *J. Virol.* 79: 11457–11466.
20. Matsutani, T., T. Yoshioka, Y. Tsuruta, S. Iwagami, and R. Suzuki. 1997. Analysis of TCRAV and TCRBV repertoires in healthy individuals by microplate hybridization assay. *Hum. Immunol.* 56: 57–69.
21. Tsuruta, Y., S. Iwagami, S. Furue, H. Teraoka, T. Yoshida, T. Sakata, and R. Suzuki. 1993. Detection of human T cell receptor cDNAs (α, β, γ and δ) by ligation of a universal adaptor to variable region. *J. Immunol. Methods* 161: 7–21.
22. Yoshida, R., T. Yoshioka, S. Yamane, T. Matsutani, T. Toyosaki-Maeda, Y. Tsuruta, and R. Suzuki. 2000. A new method for quantitative analysis of the mouse T-cell receptor V region repertoires: comparison of repertoires among strains. *Immunogenetics* 52: 35–45.
23. Horiuchi, T., M. Hirokawa, Y. Kawabata, A. Kitabayashi, T. Matsutani, T. Yoshioka, Y. Tsuruta, R. Suzuki, and A. B. Miura. 2001. Identification of the T cell clones expanding within both $CD8^+CD28^+$ and $CD8^+CD28^-$ T cell subsets in recipients of allogeneic hematopoietic cell grafts and its implication in post-transplant skewing of T cell receptor repertoire. *Bone Marrow Transplant.* 27: 731–739.
24. Hayasaka, D., N. Nagata, Y. Fujii, H. Hasegawa, T. Sata, R. Suzuki, E. A. Gould, I. Takashima, and S. Koike. 2009. Mortality following peripheral infection with tick-borne encephalitis virus results from a combination of central nervous system pathology, systemic inflammatory and stress responses. *Virology* 390: 139–150.
25. Lanteri, M. C., J. W. Heitman, R. E. Owen, T. Busch, N. Gefter, N. Kiely, H. T. Kamel, L. H. Tobler, M. P. Busch, and P. J. Norris. 2008. Comprehensive analysis of West Nile virus-specific T cell responses in humans. *J. Infect. Dis.* 197: 1296–1306.
26. Parsons, R., A. Lelic, L. Hayes, A. Carter, L. Marshall, C. Evelegh, M. Drebot, M. Andonova, C. McMurtrey, W. Hildebrand, et al. 2008. The memory T cell response to West Nile virus in symptomatic humans following natural infection is not influenced by age and is dominated by a restricted set of $CD8^+$ T cell epitopes. *J. Immunol.* 181: 1563–1572.
27. Omri, B., P. Crisanti, F. Alliot, M. C. Marty, J. Rutin, C. Levallois, A. Privat, and B. Pessac. 1994. CD4 expression in neurons of the central nervous system. *Int. Immunol.* 6: 377–385.
28. Alliot, F., M. C. Marty, D. Cambier, and B. Pessac. 1996. A spontaneously immortalized mouse microglial cell line expressing CD4. *Brain Res. Dev. Brain Res.* 95: 140–143.
29. Glass, W. G., J. K. Lim, R. Cholera, A. G. Pletnev, J. L. Gao, and P. M. Murphy. 2005. Chemokine receptor CCR5 promotes leukocyte trafficking to the brain and survival in West Nile virus infection. *J. Exp. Med.* 202: 1087–1098.
30. Liu, Y., R. V. Blanden, and A. Müllbacher. 1989. Identification of cytolytic lymphocytes in West Nile virus-infected murine central nervous system. *J. Gen. Virol.* 70: 565–573.
31. Bai, F., T. Town, F. Qian, P. Wang, M. Kamanaka, T. M. Connolly, D. Gate, R. R. Montgomery, R. A. Flavell, and E. Fikrig. 2009. IL-10 signaling blockade controls murine West Nile virus infection. *PLoS Pathog.* 5: e1000610.
32. Moore, K. W., R. de Waal Malefyt, R. L. Coffman, and A. O'Garra. 2001. Interleukin-10 and the interleukin-10 receptor. *Annu. Rev. Immunol.* 19: 683–765.
33. Cheeran, M. C., S. Hu, W. S. Sheng, A. Rashid, P. K. Peterson, and J. R. Lokensgard. 2005. Differential responses of human brain cells to West Nile virus infection. *J. Neurovirol.* 11: 512–524.
34. Zhang, B., Y. K. Chan, B. Lu, M. S. Diamond, and R. S. Klein. 2008. CXCR3 mediates region-specific antiviral T cell trafficking within the central nervous system during West Nile virus encephalitis. *J. Immunol.* 180: 2641–2649.
35. Wang, Y., M. Lobigs, E. Lee, and A. Müllbacher. 2003. $CD8^+$ T cells mediate recovery and immunopathology in West Nile virus encephalitis. *J. Virol.* 77: 13323–13334.
36. Kesson, A. M., R. V. Blanden, and A. Mullbacher. 1987. The primary in vivo murine cytotoxic T cell response to the flavivirus, West Nile. *J. Gen. Virol.* 68: 2001–2006.
37. Uren, M. F., P. C. Doherty, and J. E. Allan. 1987. Flavivirus-specific murine $L3T4^+$ T cell clones: induction, characterization and cross-reactivity. *J. Gen. Virol.* 68: 2655–2663.
38. Hill, A. B., A. Müllbacher, C. Parrish, G. Coia, E. G. Westaway, and R. V. Blanden. 1992. Broad cross-reactivity with marked fine specificity in the cytotoxic T cell response to flaviviruses. *J. Gen. Virol.* 73: 1115–1123.
39. Murali-Krishna, K., V. Ravi, and R. Manjunath. 1994. Cytotoxic T lymphocytes raised against Japanese encephalitis virus: effector cell phenotype, target specificity and in vitro virus clearance. *J. Gen. Virol.* 75: 799–807.
40. Trobaugh, D. W., L. Yang, F. A. Ennis, and S. Green. 2010. Altered effector functions of virus-specific and virus cross-reactive $CD8^+$ T cells in mice immunized with related flaviviruses. *Eur. J. Immunol.* 40: 1315–1327.
41. Dong, L., P. Li, T. Oenema, C. L. McClurkan, and D. M. Koelle. 2010. Public TCR use by herpes simplex virus-2-specific human CD8 CTLs. *J. Immunol.* 184: 3063–3071.
42. Dietrich, P. Y., F. A. Le Gal, V. Dutoit, M. J. Pittet, L. Trautman, A. Zippelius, I. Cognet, V. Widmer, P. R. Walker, O. Michielin, et al. 2003. Prevalent role of TCR α-chain in the selection of the preimmune repertoire specific for a human tumor-associated self-antigen. *J. Immunol.* 170: 5103–5109.
43. Messaoudi, I., J. LeMaoult, B. M. Metzner, M. J. Miley, D. H. Fremont, and J. Nikolich-Zugich. 2001. Functional evidence that conserved TCR CDRα3 loop docking governs the cross-recognition of closely related peptide:class I complexes. *J. Immunol.* 167: 836–843.
44. Trautmann, L., N. Labarrière, F. Jotereau, V. Karanikas, N. Gervois, T. Connerotte, P. Coulie, and M. Bonneville. 2002. Dominant TCR Vα usage by virus and tumor-reactive T cells with wide affinity ranges for their specific antigens. *Eur. J. Immunol.* 32: 3181–3190.
45. Yokosuka, T., K. Takase, M. Suzuki, Y. Nakagawa, S. Taki, H. Takahashi, T. Fujisawa, H. Arase, and T. Saito. 2002. Predominant role of T cell receptor (TCR)-α chain in forming preimmune TCR repertoire revealed by clonal TCR reconstitution system. *J. Exp. Med.* 195: 991–1001.
46. Fujii, Y., D. Hayasaka, K. Kitaura, T. Takasaki, R. Suzuki, and I. Kurane. 2011. T cell clones expressing different T cell receptors accumulate in the brains of dying and surviving mice following peripheral infection with tick-borne encephalitis virus. *Viral Immunol.* In press.

DOI: 10.1111/j.1600-0625.2012.01559.x
www.blackwellpublishing.com/EXD

Advantages of histamine H4 receptor antagonist usage with H1 receptor antagonist for the treatment of murine allergic contact dermatitis

Ayuko Matsushita[1], Masahiro Seike[1], Haruka Okawa[1], Yayoi Kadawaki[1] and Hiroshi Ohtsu[2]

[1]Department of Food and Nutrition Science, Sagami Women's Junior College, Bunkyo, Minamiku, Sagamihara, Kanagawa, Japan; [2]Department of Quantum Science and Energy Engineering, Graduate School of Engineering, Tohoku University, Aramaki, Aobaku, Sendai, Miyagi, Japan
Correspondence: Masahiro Seike, Department of Food and Nutrition Science, Sagami Women's Junior College, 2-1-1 Bunkyo, Minamiku, Sagamihara, Kanagawa 252-0383, Japan, Tel.: +81-42-749-4784, Fax: +81-42-743-4717, e-mail: m-seike@star.sagami-wu.ac.jp

Abstract: Histamine facilitates development of eczematous lesions in chronic allergic contact dermatitis. In addition to the well-known corticosteroid treatments, H1 receptor (H1R) antagonists also have been used. This study observed effects of histamine H4 receptor (H4R) antagonist usage with H1R antagonist in a murine chronic allergic contact dermatitis model, developed by repeated percutaneous challenge to the dorsal skin with 2,4,6-trinitro-1-chlorobenzene (TNCB). The H1R antagonist olopatadine hydrochloride and/or the H4R antagonist JNJ7777120 was then administered. Combination therapy was more effective than H1R antagonist monotherapy. Serum IgE and levels of interleukin (IL)-4, IL-5 and IL-6 (Th2 cytokines) in eczematous lesions decreased with combined therapy. Combined therapy with H1R and H4R antagonists counteracts the disadvantages of each as monotherapeutic agents and potentially represents a new strategy for the treatment of chronic allergic contact dermatitis.

Key words: chronic allergic contact dermatitis – H1 receptor antagonist – H4 receptor antagonist

Accepted for publication 21 June 2012

Background

Allergic contact dermatitis can cause severe and long-lasting health problems in chronically affected individuals. Repeated application of various haptens to mice induces chronic allergic lesions in the skin (1–5), and histamine facilitates development of eczematous lesions, which involves infiltration of inflammatory cells (6). H1 receptor (H1R) antagonists generally have been used as drugs for treating allergies: these also decrease the number of infiltrating cells and cytokine levels in eczematous lesions (7). In addition, H4 receptor (H4R) antagonist ameliorates eczematous lesions of murine chronic allergic contact dermatitis (8).

Questions addressed

As H1R and H4R antagonists were reported to have beneficial effects on allergic inflammation (9), this study aimed to clarify the effects of H4R antagonist usage with H1R antagonist on murine chronic allergic contact dermatitis.

Experimental design

Female C57BL/6 mice were sensitized by painting 40 μl of a 1% (in acetone) 2,4,6-trinitro-1-chlorobenzene (TNCB) solution onto the dorsal skin on experimental day 0 and were then challenged with 20 μl daily on days 7–15, and with 100 μl on day 16. The H1R antagonist olopatadine hydrochloride (olopatadine, 10 mg/kg/day) and/or the H4R antagonist JNJ7777120 (100 mg/kg/day) was orally administered 30 min before each challenge (7,8,10). On day 17, skin and blood were collected, 24 h after the final challenge (8). All experiments were performed according to the Animal Research Committee of Sagami Women's University guidelines for the care and use of experimental animals.

Results

Marked epidermal hyperplasia with intercellular oedema and intense dermal cell infiltration was observed after the repeated challenge (Fig. 1a,b). These eczematous-like lesions were ameliorated by olopatadine (Fig. 1c), olopatadine and JNJ7777120 (Fig. 1d), or JNJ7777120 (Fig. 1e). Epidermal thickness in this model was significantly decreased by combined therapy or JNJ7777120 alone, but was not significantly changed by olopatadine monotherapy (Fig. 1f). The number of eosinophils was significantly decreased by olopatadine or JNJ7777120 and was further decreased by their combination as compared to olopatadine alone (Fig. 1g). The number of mast cells was significantly decreased by JNJ7777120 and was not further changed by combination therapy (Fig. 1h). JNJ7777120 monotherapy and the combination reduced the numbers of eosinophils and mast cells to a similar extent (Fig. 1g,h).

Serum IgE and skin levels of IL-4, IL-5 and IL-6 (representative Th2 cytokines) were increased in this model (Fig. 2a–d). Serum IgE was decreased significantly by olopatadine or JNJ7777120 monotherapy. Skin IL-4 level was decreased significantly by JNJ7777120 monotherapy. Combined therapy further decreased serum IgE and IL-4 compared to olopatadine or JNJ7777120 monotherapy (Fig. 2a,b). IL-5 was decreased by olopatadine or JNJ7777120 monotherapy, and combined therapy was not more effective (Fig. 2c). IL-6 was not significantly changed by olopatadine monotherapy, but was significantly decreased by combined therapy (Fig. 2d); however, combined therapy was not further effective compared to JNJ7777120 monotherapy (Fig. 2d). Skin levels of IFN-gamma and IL-12 (representative Th1 cytokines) were also increased by the repeated challenge (Fig. 2e,f) and tended to be reduced by olopatadine and increased by JNJ7777120 (Fig. 2e,f); addition of olopatadine negated this JNJ7777120 effect (Fig. 2e,f).

Discussion

It was expected that the newly developed H4R antagonists would be useful for the treatment of allergic diseases (9). JNJ7777120 is a high-affinity H4R antagonist and exhibits only low affinity for H1R, H2R and H3R (11). Previously we observed the effect of JNJ7777120 on chronic allergic contact dermatitis in mice and the effect of the H4R agonist 4-methylhistamine on histidine

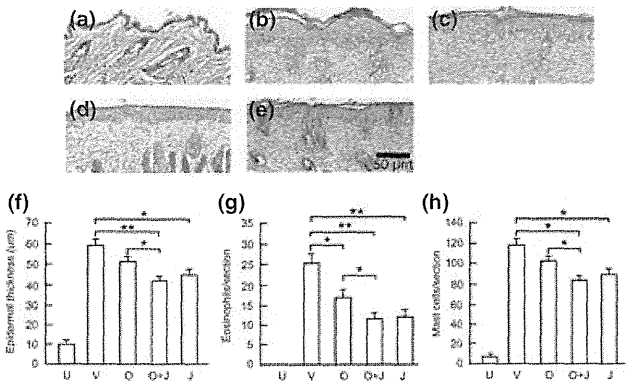

Figure 1. Effects of olopatadine and JNJ7777120 administrations on eczematous lesions and numbers of infiltrated eosinophils and mast cells in murine allergic contact dermatitis. (a–e) Histology of skin lesions (haematoxylin and eosin staining) after sensitization and repeated challenge. (a) Unchallenged. (b) Challenge + vehicle (methyl cellulose and hydroxypropyl-β-cyclodextrin solution). (c) Challenge + olopatadine (suspended in 0.5% methyl cellulose solution). (d) Challenge + olopatadine + JNJ7777120 (suspended in 20% hydroxypropyl-β-cyclodextrin solution). (e) Challenge + JNJ7777120. (f) Epidermal thickness and numbers of (g) eosinophils and (h) mast cells in eczematous lesions. Mean ± SEM (n = 7). *P < 0.05, **P < 0.01 by Holm's multiple comparison test. The other comparison excluding the value for the unchallenged mice group was not statistically significant. U, unchallenged; V, challenge + vehicle; O, challenge + olopatadine; O + J, challenge + olopatadine + JNJ7777120; J, challenge + JNJ7777120. Epidermal thickness and eosinophils and mast cell numbers were obtained according to the previous publication (6, 18).

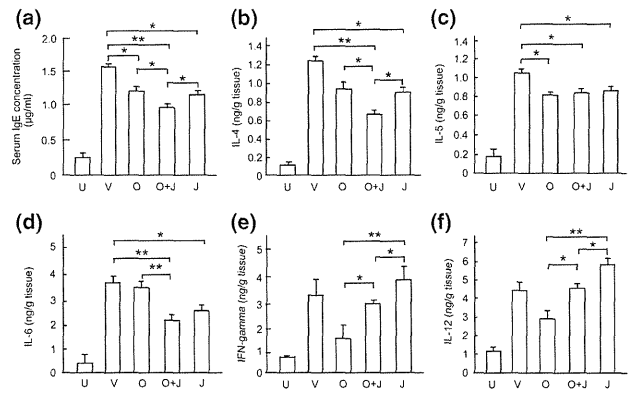

Figure 2. Effects of olopatadine and JNJ7777120 administration on serum IgE and tissue cytokines. (a) Serum IgE. (b) IL-4. (c) IL-5. (d) IL-6. (e) IFN-gamma. (f) IL-12. Mean ± SEM (n = 7). *P < 0.05, **P < 0.01 by Holm's multiple comparison test. The other comparison excluding the value for the unchallenged mice group was not statistically significant. U, unchallenged; V, challenge + vehicle; O, challenge + olopatadine; O + J, challenge + olopatadine + JNJ7777120; J, challenge + JNJ7777120. A skin sample was homogenized in PBS, and levels of cytokines in the supernatant were determined by ELISA (Ray Biotech Inc., Norcross, GA) (8). Serum IgE was measured using an ELISA kit (Shibayagi Inc., Gunma, Japan).

decarboxylase (−/−) mice (which produce no histamine), to confirm JNJ7777120 as an H4R antagonist (8); however, this activity was not apparent at doses <100 mg/kg. As JNJ7777120 had recently been thought to produce antagonist and partial agonist effects (12), that report provided important support for the role of JNJ7777120 as an H4R antagonist in the murine chronic allergic contact dermatitis model. In that report, because H4R agonist and H4R antagonist agents were used, the observed opposite effects of JNJ7777120 on Th1 and Th2 cytokines could have been exerted through intracellular mechanisms.

In this study, eczematous lesions were ameliorated, and the numbers of mast cells and eosinophils were decreased by the administration of H1R and/or H4R antagonists. Histamine, acting through H4R, induces chemotaxis of murine eosinophils (13) and mast cells (14). The current results demonstrate that concurrent administration of H1R and H4R antagonists did not further suppress the migration of eosinophils and mast cells to a significant extent. A previously reported study demonstrated that concurrent administration of H1R and H4R antagonists did not significantly alter eosinophil accumulation in BAL fluid (15). Therefore, it is suggested that the chemotactic role of histamine for eosinophils occurs mainly through the H4R.

Combined therapy with H1R and H4R antagonists decreased serum IgE and Th2 cytokines more than monotherapy with the H1R antagonist and was therefore more beneficial. As the Th1 cytokines IFN-gamma and IL-12 have been reported to accelerate the process of allergic dermatitis (16), monotherapy with H4R antagonist is disadvantageous in this regard; however, combination therapy could solve this problem.

Considering all these facts together, we propose that combined therapy might be more beneficial than monotherapy with H1R or H4R antagonist for management of allergic diseases, including contact dermatitis and atopic dermatitis. As marked strain-related differences are reported for the pharmacological activity of JNJ7777120 in skin inflammation (17), careful consideration should be given to the application of these preclinical data in the human clinical setting.

Acknowledgements

Ayuko Matsushita, Masahiro Seike and Hiroshi Ohtsu designed the research study and wrote the paper. Ayuko Matsushita, Haruka Okawa and Yayoi Kadowaki performed the research and analysed the data. We thank Kyowa Hakko Kirin for providing olopatadine and Johnson & Johnson Pharmaceutical Research & Development for donating JNJ7777120. This work was supported by a grant-in-aid from the Ministry of Education, Science and Culture of Japan.

Conflict of interests

The authors have declared no conflicting interests.

References

1 Kitagaki H, Fujisawa S, Watanabe K *et al.* J Invest Dermatol 1995: **105**: 749–755.
2 Kitagaki H, Ono N, Hayakawa K *et al.* J Immunol 1997: **159**: 2484–2491.
3 Seike M, Ikeda M, Kodama H *et al.* Exp Dermatol 2005: **14**: 169–175.
4 Weise C, Zhu Y, Ernst D *et al.* Exp Dermatol 2011: **20**: 805–809.
5 Röse L, Schneider C, Stock C *et al.* Exp Dermatol 2011: **21**: 25–31.
6 Seike M, Takata T, Ikeda M *et al.* Arch Dermatol Res 2005: **297**: 68–74.
7 Hamada R, Seike M, Kamijima R *et al.* Eur J Pharmacol 2006: **547**: 45–51.
8 Seike M, Furuya K, Omura M *et al.* Allergy 2010: **65**: 319–326.
9 Thurmond R L, Gelfand E W, Dunford P J. Nat Rev Drug Discov 2008: **7**: 41–53.
10 Dunford P J, Williams K N, Desai P J *et al.* J Allergy Clin Immunol 2007: **119**: 176–183.
11 Venable J D, Thurmond R L. Antiinflamm Antiallergy Agents Med Chem 2006: **5**: 307–322.
12 Seifert R, Schneider E H, Dove S *et al.* Mol Pharmacol 2011: **79**: 631–638.
13 Ling P, Ngo K, Nguyen S *et al.* Br J Pharmacol 2004: **142**: 161–171.
14 Hofstra C L, Desai P J, Thurmond R L *et al.* J Pharmacol Exp Ther 2003: **305**: 1212–1221.
15 Deml K F, Beermann S, Neumann D *et al.* Mol Pharmacol 2009: **76**: 1019–1030.
16 Hamid Q, Boguniewicz M, Leung D Y. J Clin Invest 1994: **94**: 870–876.
17 Coruzzi G, Pozzoli C, Adami M *et al.* Exp Dermatol 2012: **21**: 32–37.
18 Cameron G S, Pence B C. J Invest Dermatol 1992: **99**: 189–192.

Allergy EUROPEAN JOURNAL OF ALLERGY AND CLINICAL IMMUNOLOGY

Allergy

ORIGINAL ARTICLE EXPERIMENTAL ALLERGY AND IMMUNOLOGY

The antagonism of histamine H1 and H4 receptors ameliorates chronic allergic dermatitis via anti-pruritic and anti-inflammatory effects in NC/Nga mice

Y. Ohsawa & N. Hirasawa

Laboratory of Pharmacotherapy of Life-Style Related Diseases, Graduate School of Pharmaceutical Sciences, Tohoku University, Sendai, Japan

To cite this article: Ohsawa Y, Hirasawa N. The antagonism of histamine H1 and H4 receptors ameliorates chronic allergic dermatitis via anti-pruritic and anti-inflammatory effects in NC/Nga mice. *Allergy* 2012; **67:** 1014–1022.

Keywords
atopic dermatitis; histamine H1 receptor; histamine H4 receptor; keratinocytes; mast cells.

Correspondence
Yusuke Ohsawa, Laboratory of Pharmacotherapy of Life-Style Related Diseases, Graduate School of Pharmaceutical Sciences, Tohoku University, Sendai, Japan.
Tel.: +81-22-795-5915
Fax: +81-22-795-5504
E-mail: yuusuke_oosawa@pharm.kissei.co.jp

Accepted for publication 01 May 2012

DOI:10.1111/j.1398-9995.2012.02854.x

Edited by: Angela Haczku

Abstract

Background: Although histamine H1 receptor (H1R) antagonists are commonly used to treat atopic dermatitis, the treatment is not always effective. The histamine H4 receptor (H4R) was recently described as important to the pruritus in dermatitis. Here, we investigated whether the combination of a H1R antagonist plus a H4R antagonist attenuates chronic dermatitis in NC/Nga mice.
Methods: Chronic dermatitis was developed by repeated challenges with picryl chloride on the dorsal back and ear lobes. The therapeutic effects of the H1R antagonist olopatadine and H4R antagonist JNJ7777120 on scratching and the severity of dermatitis were evaluated. In addition, the mechanisms responsible for the anti-allergic effects of H1R and/or H4R antagonism were examined using bone marrow-derived mast cells (BMMC) and keratinocytes.
Results: JNJ7777120 attenuated scratching behavior after a single administration and improved dermatitis, as assessed with clinical scores, pathology, and cytokine levels in skin lesions when administered repeatedly. These effects were augmented by combined treatment with olopatadine, having a similar therapeutic efficacy to prednisolone. JNJ7777120 inhibited dose-dependently the production of thymus and activation-regulated chemokine/CCL17 and macrophage-derived chemokine/CCL22 from antigen-stimulated BMMC. In addition, olopatadine reversed the histamine-induced reduction of semaphorin 3A mRNA in keratinocytes.
Conclusion: Combined treatment with H1R and H4R antagonists may have a significant therapeutic effect on chronic dermatitis through the synergistic inhibition of pruritus and skin inflammation.

Atopic dermatitis (AD) is an allergic inflammatory disease characterized by intense pruritus, chronic eczematous plaques, and relapsing inflammation induced by repeated exposure to an antigen. The inflamed skin contains mast cells, eosinophils, and Th2 cells and exhibits histological abnormalities such as scaling, crusting, and lichenoid papules (1, 2). The cytokine milieu of the inflamed skin shows Th2-dominant responses indicated by production of IL-4, IL-5, and IL-13 (2). These responses are triggered by thymic stromal lymphopoietin (TSLP) produced by keratinocytes (3).

Vigorous pruritus is the most important issue for a therapeutic strategy in patients with AD, and the pruritus associated with AD is poorly controlled clinically and affects the quality of life of patients. Histamine has been extensively studied for its pruritogenic effects (4, 5). It has been shown to be a potent pruritogen when applied to both human normal skin (6) and diseased skin (7). However, there is no clear evidence that histamine H1 receptor (H1R) antagonists inhibit it.

Four types of histamine receptors have been identified to date. The fourth, the histamine H4 receptor (H4R), which

Abbreviations
AD, atopic dermatitis; BMMC, bone marrow-derived mast cells; H1R, histamine H1 receptor; H4R, histamine H4 receptor; HDC, histidine decarboxylase; MDC, macrophage-derived chemokine; NGF, nerve growth factor; PiCl, picryl chloride; Sema3A, semaphorin 3A; TARC, thymus and activation-regulated chemokine; TSLP, thymic stromal lymphopoietin.

was cloned in 2000, is expressed on several hematopoietic cells and plays important roles in the activation of mast cells, eosinophils, monocytes, dendritic cells, and T cells (8–11). Thus, H4R is considered a new therapeutic target for allergic inflammation in case of AD, asthma, and rhinitis (12–15). Using H4R-deficient mice or a H4R antagonist, it has been indicated that H4R plays roles in pruritus and acute inflammation (12, 13, 16–19). Previously, we examined the inhibitory effects of anti-histamines, which include pyrilamine, an H1R antagonist, cimetidine, an H2R antagonist, and thioperamide, an H3R/H4R antagonist on TPA-enhanced picryl chloride (PiCl)-induced allergic dermatitis in mice (12). As the results, we found that the H2R antagonist showed only a slight inhibition. In contrast, the H1R antagonist significantly inhibited the increase in the ear thickness in the early phase and the H3R/H4R antagonist significantly inhibited the delayed phase responses such as eosinophil infiltration, and the combination of the H1R antagonist and the H3R/H4R antagonist showed additive effects.

As far, there were several trials of the combination of H1R antagonist and H2R antagonist on AD, which indicated no benefit (20). Here, we investigated whether or not a H4R antagonist or H4R plus H1R antagonist inhibits chronic allergic dermatitis in NC/Nga mice. The mechanisms of anti-allergic function via the inhibition of H4R and/or H1R were also verified *in vitro*.

Materials and methods

Animals

Male NC/Nga mice (specific pathogen-free) aged 6 weeks were purchased from Japan SLC. All mice were treated in accordance with procedures approved by the local Animal Ethics Committee.

Sensitization and repeated challenge

For sensitization, 150 μl of a 5% (w/v) picryl chloride (Nacalai tesque, Kyoto, Japan) solution (3 : 1 in acetone/ethanol) was applied using a micropipette to the thoracic and abdominal areas. Five days later, the first challenge was performed by applying 200 μl of a 1.2% (w/v) PiCl solution in olive oil, to the back and to the left and right ears. This procedure was repeated once a week for up to 10 weeks.

Drugs

Olopatadine (3 mg/kg; AK scientific, Union, CA, USA), JNJ7777120 (30 mg/kg; provided by Johnson & Johnson Pharmaceutical Research & Development, L.L.C., San Diego, CA, USA), and prednisolone (3 mg/kg; Sigma-Aldrich, St. Louis, MO, USA) were suspended in 0.5% carboxyl methylcellulose and administered orally in a volume of 5 ml/kg every other day from 5 to 10 weeks after the sensitization. The doses of these histamine antagonists were selected according to the previous reports (16, 18, 21, 22). For *in vitro* experiments, histamine antagonists were dissolved in DMSO and the final concentration of DMSO was adjusted to 0.1–0.2%.

Real-time PCR for histidine decarboxylase (HDC) and measurement of plasma levels of histamine

Forty-eight hours after the fifth challenge at 5 weeks, blood and the ear lobes were collected. The level of histamine in plasma was determined using a Histamine EIA kit (SPI-Bio, Montigny le Bretonneux, France), and total RNA of the tissues was extracted using an RNeasy Fibrous Tissue Kit (Qiagen, Hilden, Germany). The primers for real-time PCR were (forward) 5′-TGTGTCCGTCGTGGATCTGA-3′ and (Reverse) 5′-TTGCTGTTGAAGTCGCAGGAG-3′ for mouse GAPDH, and (forward) 5′-TCCATTAAGCTGTGGTTTGTGATTC-3′ and (reverse) 5′-CGCTTCTGACCAGAGATTCAAAGTA-3′ for mouse HDC.

Counting of scratching and scoring of dermatitis

Three days after the fifth challenge, the number of times the mice scratched during 2 h after receiving a single drug dose was counted and then the severity of the dermatitis was evaluated once a week from week 5 to 10 following repeated treatment. The observation items were (I) flare and hemorrhage, (II) edema, (III) excoriation and erosion, and (IV) incrustation and xerosis. Evaluation items were scored as follows: 0 = no sign; 1 = mild; 2 = moderate; 3 = severe. The sum of the scores for each evaluation item (maximum score: 12) was taken as the dermatitis score.

Histological analysis

Ten weeks after the sensitization, the ear lobe was excised and paraffin-embedded sections were prepared. Serial sections were stained with hematoxylin–eosin or 0.05% toluidine blue. $CD4^+$ helper T cells were immunostained with anti-mouse CD4 antibody (R&D systems, Minneapolis, MN, USA).

Measurement of levels of cytokines in skin lesions and IgE in plasma

Ten weeks after the sensitization, the ear lobe was immersed in liquid nitrogen, crushed with an SK Mill (Tokken, Kashiwa, Japan), and suspended in 1 ml of PBS containing a protease inhibitor (Complete™; Roche Diagnostics, Mannheim, Germany). The suspension was centrifuged at 1200 ***g*** for 10 min, and the supernatants of tissue homogenates and the plasma were used to analyze the levels of IL-4, IL-5, TSLP (Biolegend, San Diego, CA, USA), thymus and activation-regulated chemokine (TARC) (R&D systems), nerve growth factor (NGF) (Promega, Madison, WI, USA), and plasma IgE (Biolegend) with ELISA kits.

Preparation of bone marrow-derived mast cells

Bone marrow-derived mast cells (BMMC) were prepared from the bone marrow cells aspirated from NC/Nga mice (6–8 weeks old). The bone marrow cells were cultured in RPMI1640 medium that contained 10% FBS, HEPES (25 mM), penicillin (100 units/ml), streptomycin (100 μg/ml),

and recombinant mIL-3 (300 pg/ml; R&D systems) for 9 days. More than 80% of bone marrow cells were positive for FcεRI and c-kit, as assessed by flow cytometric analysis with PE-labeled anti-mouse FcεRI antibody (Biolegend) and FITC-labeled anti-mouse c-kit antibody (Biolegend).

Stimulation of BMMC with anti-DNP IgE and DNP-BSA, and measurement of levels of thymus and activation-regulated chemokine (TARC/CCL17) and macrophage-derived chemokine (MDC/CCL22)

Bone marrow-derived mast cells were primed overnight with anti-DNP IgE (0.5 μg/ml; Sigma-Aldrich). The cells were treated with olopatadine and/or JNJ7777120 for 30 min and then stimulated with DNP-BSA (1–25 ng/ml; LSL, Japan) for 24 h. The amount of histamine in the culture medium was determined by EIA, and TARC and MDC levels were measured with ELISA kits (R&D systems).

Change of semaphorin 3A (Sema3A) mRNA levels after histamine treatment in PAM212 cells

PAM 212, a murine keratinocyte cell line, kindly supplied by Dr. S. H. Yuspa, NCI, NIH, USA, was cultured in RPMI1640 medium containing 10% FBS, penicillin (100 units/ml), streptomycin (100 μg/ml), and HEPES (25 mM). The cells were incubated for 30 min in medium containing olopatadine and then stimulated with histamine at various concentrations. The level of mRNA for Sema3A was evaluated by real-time PCR. The primers for PCR were (forward) 5′-AGATGCTCCATTCCAGTTTGTTCAC-3′ and (Reverse) 5′-ACATAAGCCACCGCATCACTTGTA-3′ for mouse Sema3A.

Statistical significance

Values are presented as the standard error of the mean. The statistical significance of the results was analyzed with the Student's *t*-test, Dunnett's test for parametric analysis, or corresponding to score for nonparametric analysis.

Results

Increased histamine production and release in mice with PiCl-induced chronic dermatitis

The NC/Nga mice treated with PiCl for 5 weeks developed moderate dermatitis with erythema, crusting and skin erosion on the treated skin and ear lobes (Fig. 1B) compared with intact mice (Fig. 1A). Forty-eight hours after the fifth treatment, the level of histamine in plasma (Fig. 1C) and the level of HDC mRNA in skin lesions (Fig. 1D) were significantly increased.

Effects of single administration of olopatadine and JNJ7777120 on scratching behavior

Three days after the fifth challenge, drugs were administered and scratching counts were determined. As shown in Fig. 1E, the number of times the mice scratched during 2 h was significantly increased. Administration of olopatadine or JNJ7777120 apparently reduced the counts, and combined treatment significantly decreased them. The anti-pruritus effect of the combined treatment was as potent as that of prednisolone.

Amelioration of dermatitis by repeated administration of olopatadine and JNJ7777120

Olopatadine and/or JNJ7777120 were administered every other day after the fifth treatment with PiCl, and the dermatitis score was evaluated until week 10. The dermatitis score progressively increased dependent on the number of challenges with PiCl. JNJ7777120, but not olopatadine, prevented this increase (Fig. 1F). Interestingly, combined treatment had a significant effect from 8 weeks (Fig. 1F), and the severity of the dermatitis was reduced about 50% compared with the control group at 10 weeks. Consistent with the anti-pruritic effects, dual inhibition of H1R and H4R was as effective as prednisolone.

Effects of repeated administration of olopatadine and JNJ7777120 on histological changes and the number of mast cells

Histological examination revealed that the repeated treatment with PiCl caused severe acanthosis and the infiltration by inflammatory cells including lymphocytes and eosinophils of the ear lobe (Fig. 2B, E). The number of mast cells also increased significantly (Fig. 2G, I). Combined treatment with olopatadine and JNJ7777120 improved the hyperepidermis (Fig. 2C, F). JNJ7777120 decreased the number of mast cells (Fig. 2H, I). Olopatadine alone did not decrease but augmented the inhibitory effects of JNJ7777120 (Fig. 2I).

Effects of repeated administration of olopatadine and JNJ7777120 on levels of cytokines in tissue and IgE in plasma

Next, we assessed the levels of IL-4, IL-5, TSLP, TARC, and NGF in tissue, and IgE in plasma at 10 weeks after the sensitization. Olopatadine decreased the level of NGF but not IL-4, IL-5, TSLP, TARC, or IgE (Fig. 3). In contrast, JNJ7777120 not only significantly decreased the NGF levels but also markedly inhibited the increases in IL-4, IL-5, TSLP, and TARC (Fig. 3). Although neither olopatadine nor JNJ7777120 alone reduced the plasma IgE level, in combination they inhibited the increase in IgE level similar to prednisolone (Fig. 3F). The production of MDC in tissue was not significantly inhibited by olopatadine, JNJ7777120, and prednisolone (data not shown).

Effects of olopatadine and JNJ7777120 on production of TARC and MDC in BMMC

To analyze the mechanism behind the anti-inflammatory effects of H1R and H4R antagonists, we tested whether olopatadine and/or JNJ7777120 inhibit TARC and MDC

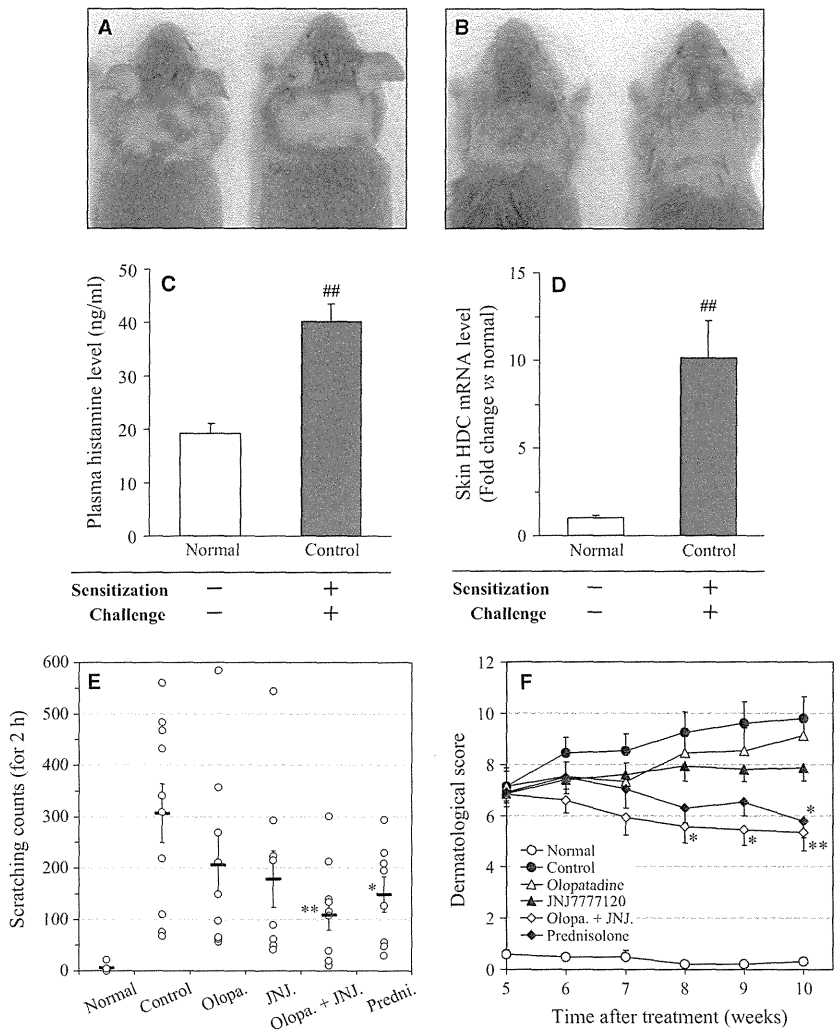

Figure 1 Increased histamine levels in picryl chloride (PiCl)-induced chronic allergic dermatitis and effects of olopatadine and JNJ7777120 on scratching counts and dermatological scores. NC/Nga mice were sensitized and challenged as described in 'Materials and Methods'. Forty-eight hours after the challenge, mice of the normal group (intact mice, A) and control group (PiCl-sensitized and challenged mice, (B) were photographed. The levels of histamine in plasma (C) and histidine decarboxylase (HDC) mRNA in the inflamed skin (D) were determined. Three days after the fifth challenge, mice were orally administered olopatadine (3 mg/kg), JNJ7777120 (30 mg/kg), olopatadine plus JNJ7777120, or prednisolone (3 mg/kg), and then, scratching counts for 2 h were determined (E). The severity of the dermatitis was scored once a week from week 5 to 10 during repeated administration (F). Statistical significance; $^{\#\#}P < 0.01$ *vs* normal group ($n = 4$), $^{*}P < 0.05$ and $^{**}P < 0.01$ *vs* control group ($n = 6$–10).

produced by BMMC. Bone marrow cells prepared from NC/Nga mice were induced to differentiate into FcεRI^{+}/c-kit^{+} mast cells (more than 80%) over 9 days (Fig. 4A). The stimulation of BMMC with the antigen increased the levels of histamine (Fig. 4B), TARC, and MDC (Fig. 4C) in the medium collected at 24 h. The histamine release was slightly inhibited by olopatadine at 10 μM (about 16% inhibition) but not JNJ7777120 at 30 μM (data not shown). The production of TARC and MDC was inhibited slightly by olopatadine at 10 μM and significantly by JNJ7777120 in a dose-dependent manner (30–100 μM) (Fig. 4C). The H3R/H4R antagonist thioperamide (100 μM) also suppressed the production of TARC (Fig. 4D). Furthermore, JNJ7777120 plus olopatadine inhibited additively TARC production (Fig. 4D). It was unlikely that JNJ7777120 reduced the production of these cytokines via toxic effects because JNJ7777120 did not reduce the antigen-induced release of IL-13 (data not shown).

Consistent with the reduction in TARC and MDC production in BMMC, the infiltration of CD4-positive cells in the skin 10 weeks after the sensitization was decreased by the combined treatment with olopatadine and JNJ7777120 (Fig. 4E, F).

Effects of olopatadine on histamine-induced down-regulation of Sema3A expression in PAM212 cells

Finally, we tested whether olopatadine and/or JNJ7777120 affect the level of mRNA for Sema3A, the regulatory